Title: Shifts in the Isotopic Composition of Nitrous Oxide between El Niño and La Niña in the Eastern Tropical South Pacific

Noah Gluschankoff[1], Alyson E. Santoro[2], Carolyn Buchwald[3], and Karen L. Casciotti[1,4]

[1]Stanford University, Department of Earth System Science, Stanford, CA, USA

[2]University of California, Department of Ecology, Evolution and Marine Biology, Santa Barbara, CA USA

[3]Dalhousie University, Department of Oceanography, Halifax, Nova Scotia, Canada

[4]Stanford University, Oceans Department, Stanford, CA, USA

Keywords: Nitrous Oxide, Isotopes, El Niño, Upwelling

Key Points:

1. La Niña in the Eastern Tropical South Pacific led to a six-fold increase in nitrous oxide concentrations compared to El Niño.
2. Isotopocule analysis indicates incomplete denitrification and hybrid production both contributed to the accumulation of nitrous oxide.
3. Numerous co-occurring production and consumption pathways likely explain the nitrous oxide distributions.

Abstract

The El Niño-Southern Oscillation (ENSO) is a natural climate phenomenon that alters the biogeochemical and physical dynamics of the Eastern Tropical Pacific Ocean. Its two phases, El Niño and La Niña, are characterized by decreased and increased coastal upwelling, respectively, which have cascading effects on primary productivity, organic matter supply, and ocean-atmosphere interactions. The Eastern Tropical South Pacific (ETSP) oxygen minimum zone (OMZ) is a source of nitrous oxide (N_2O), a potent greenhouse gas, to the atmosphere. While nitrogen cycling in the ETSP OMZ has been shown to be sensitive to ENSO, we present the first study to directly compare N_2O distributions during both ENSO phases using N_2O isotopocule analyses. Our data show that during La Niña, N_2O accumulation increased six-fold in the upper 100 m of the water column, and N_2O fluxes to the atmosphere increased up to 100-fold. N_2O isotopocule data demonstrated substantial increases in $\delta^{18}O$ up to 60.5‰ and decreases in $\delta^{15}N^{\beta}$ down to -10.3‰, signaling a shift in N_2O cycling during La Niña in the oxycline compared to El Niño.

N_2O production via the hybrid pathway and incomplete denitrification with overprinting of N_2O consumption are likely co-occurring to maintain the high site preference (SP) values (17‰ – 26.7‰), corroborating previous hypotheses. Ultimately, our results illustrate a strong connection between upwelling intensity, biogeochemistry, and N_2O flux to the atmosphere, and highlight the importance of repeat measurements in the same region to constrain N_2O interannual variability and cycling dynamics under different climate scenarios.

Plain Language Summary

Nitrous oxide is a greenhouse gas that is 300 times more potent than carbon dioxide in its ability to warm Earth, and it can be produced and consumed through the activities of microorganisms in the ocean. The low-oxygen waters of the Eastern Tropical South Pacific are a known global 'hotspot' for nitrous oxide cycling, as the chemical and physical conditions there provide fuel for nitrous oxide production. A natural climate cycle known as the El Niño-Southern Oscillation, which has a warm and cold phase, can affect the conditions that raise or lower the speed of nitrous oxide cycling. We used isotopes – small, but measurable natural differences in the masses of molecules and atoms – to understand how nitrous oxide cycling changes during each phase. We found a decrease in nitrous oxide accumulation during the warm phase, and enhanced production during the cold phase. This enhanced production is connected to more nitrous oxide being released to the atmosphere from the ocean during the cold phase.

Acknowledgments, Samples, and Data

The authors would like to thank the captain and crew of the R/V *Atlantis* and R/V *Melville*, as well as chief scientists A. Knapp, W. Berelson, and D. Capone. The authors thank M. McIlvin and M. Forbes for their technical support of the isotopic measurements and C. L. Kelly for their helpful discussions. This research was supported by National Science Foundation award OCE-0961098 to K. L. Casciotti. N. Gluschankoff is supported by a Graduate Research Assistantship from Stanford University. The authors declare no competing financial interests. The manuscript is prepared to comply with the AGU data policy. The data reported in this study can be found in the Stanford Digital Repository (https://purl.stanford.edu/sc709fd6894; Gluschankoff et al., 2022) and has been submitted to BCO-DMO.

1. Introduction

Nitrous oxide (N_2O) is a powerful greenhouse gas naturally formed in the ocean via microbial processes. N_2O has a greenhouse warming potential up to 300 times that of carbon dioxide (CO_2) on a per molecule basis, and is also the most prominent chemical agent contributing to the depletion of stratospheric ozone (Crutzen, 1970; Ravishankara et al., 2009). Global emissions of N_2O are dominated by terrestrial sources such agriculture and natural emissions from soils, however approximately 20% of all N_2O emitted to the atmosphere is derived from natural processes in marine environments (Thompson et al., 2014, 2019; Tian et al., 2020). Of those marine environments, regional oxygen (O_2) minimum zones (OMZs) and eastern boundary upwelling systems, such as the Eastern Tropical South Pacific (ETSP), are among the most significant sources of N_2O (Arévalo-Martínez et al., 2015; Nevison et al., 2004; Yang et al., 2020).

A characteristic OMZ includes a shallow, well ventilated mixed layer, underlain by a steep decreasing O_2 gradient, known as the oxycline, where N_2O is rapidly produced (Farías et al., 2009; Frey et al., 2020; Ji et al., 2015). Below the oxycline is the oxygen deficient zone (ODZ), a region of functional anoxia where fixed nitrogen is removed by denitrification and anammox (Bourbonnais et al., 2015; Cohen & Gordon, 1978; Kuypers et al., 2005; Ward et al., 2009), and N_2O is reduced to nitrogen gas (N_2) (Babbin et al., 2015; Bulow et al., 2010; Sun et al., 2020). It is at the oxic-anoxic boundary found between the base of the oxycline and the ODZ where the most intense N_2O cycling occurs, as N_2O can be both produced by nitrification and denitrification, and also consumed by denitrification (Bourbonnais et al., 2017; Casciotti et al., 2018).

Denitrification is the anaerobic stepwise reduction of nitrate (NO_3^-) or NO_2^- to nitrogen gas (N_2) via nitric oxide (NO) and N_2O. When the process does not go to completion, it can produce N_2O at high rates. The enzymes responsible for each step in denitrification are increasingly sensitive to dissolved O_2 concentrations, thus, incomplete denitrification can produce N_2O when nitrous oxide reductase is inhibited by the presence of dissolved O_2 (Bonin et al., 1989). It is thought that denitrification produces N_2O at rates up to 2 orders of magnitude higher than nitrification in the suboxic ocean ($[O_2]<20$ μM; Babbin et al., 2015; Frey et al., 2020; Ji et al., 2015). In the functionally anoxic regions ($[O_2]<5$ μM) of the water column, consumption of N_2O via denitrification dominates its cycling, leading to a local minima in N_2O concentration, but N_2O production may continue to occur (Casciotti et al., 2018; Cohen & Gordon, 1978; Elkins et al., 1978; Kelly et al., 2021; Monreal et al., 2022; Sun et al., 2020; Suntharalingam & Sarmiento, 2000).

In oxic waters, N_2O production is largely linked to nitrification (Elkins et al., 1978; Nevison et al., 2003; Yoshinari, 1976), and it is recognized that ammonia-oxidizing archaea (AOA) represent the dominant oceanic nitrifiers and sources of N_2O in the oxygenated ocean (Francis et al., 2005; Frey et al., 2020; Santoro et al., 2011; Toyoda et al., 2019). AOA may produce N_2O through multiple pathways, including a putative "hybrid mechanism," combining nitrogen atoms sourced from ammonium (NH_4^+) – derived from the degradation of organic matter – and from nitrite (NO_2^-) to produce N_2O (Frame et al., 2017; Frey et al., 2020; Kozlowski et al., 2016; Löscher et al., 2012; Santoro et al., 2011; Stein, 2019; Stieglmeier et al., 2014). Rates of hybrid N_2O production appear to represent more than 70% of N_2O produced from NH_4^+ in OMZs (Frey et al., 2020; Ji et al., 2015; Santoro et al., 2021). Ammonia-oxidizing bacteria (AOB) may also produce N_2O, but the role AOB play in oceanic N_2O production appears to be small (Francis et al., 2005; Löscher et al., 2012; Santoro et al., 2010). The N_2O yields from AOA and AOB have been shown to increase under high NO_2^- and low O_2 concentrations (Frame & Casciotti, 2010; Frey et al., 2020; Ji et al., 2018; Löscher et al., 2012; Santoro et al., 2021). Thus, organisms involved with both nitrification and denitrification can produce N_2O at significant rates in suboxic waters; however, their relative contributions on a global scale remain unresolved (Martinez-Rey et al., 2015).

Of the ocean's three primary OMZs, the ETSP OMZ is believed to be the single largest natural oceanic source of N_2O, and its biogeochemical dynamics are sensitive to interannual variability, such as the El Niño-Southern Oscillation (ENSO; Ji et al., 2019; Llanillo et al., 2013; Yang et al., 2017, 2020). ENSO oscillates approximately every two to seven years and shifts the spatial distribution of biologically limiting nutrients, dissolved O_2, and microbial community composition in the equatorial Pacific Ocean through alterations to the dominant ocean circulation patterns (Espinoza-Morriberón et al., 2019; Llanillo et al., 2013; Mogollón & Calil, 2017). These shifts in ocean circulation modulate the ventilation of the upper ocean and organic matter supply in the tropical Pacific Ocean, which in turn, alters the cycling and emissions of N_2O (Babbin et al., 2020; Espinoza-Morriberón et al., 2019; Ji et al., 2019; Mogollón & Calil, 2017; Thompson et al., 2014). In climate model simulations, the more oxic conditions and decreased organic matter (OM) supply in near-shore waters of the ETSP OMZ during El Niño have been predicted to decrease the rates of suboxic processes like denitrification, which could decrease overall N_2O production and consumption (Mogollón & Calil, 2017; Yang et al., 2017). The opposite scenario would be expected during La Niña, with an expanded ODZ volume and increased OM supply increasing N_2O production and consumption in the oxycline and ODZ, respectively (Yang et al., 2017).

Projections of increased ocean deoxygenation, as well as increased frequency and intensity of ENSO events, have significant implications for ocean biogeochemistry with potential repercussions to N_2O cycling and emissions to the atmosphere (Babbin et al., 2020; Cai et al., 2014, 2015; Horak et al.,

2016; Schmidtko et al., 2017; Stramma et al., 2008; Yang et al., 2017). The distinct oceanographic conditions observed during both phases of ENSO can be harnessed as natural experiments of modified ocean biogeochemistry and circulation. We hypothesized that the expanded low oxygen waters, enhanced upwelling, and greater substrate availability in shallower waters during La Niña, compared to El Niño, could increase the overall production of N_2O through both denitrification and nitrification in the oxycline, and increase the N_2O flux to the atmosphere.

N_2O is composed of numerous isotopocules, molecules that differ only in their isotopic composition. As N has two stable isotopes, ^{14}N and ^{15}N, and O has three stable isotopes, ^{16}O, ^{17}O, and ^{18}O, the primary isotopocules of N_2O are ^{14}N-^{14}N-^{16}O, ^{15}N-^{14}N-^{16}O, ^{14}N-^{15}N-^{16}O, ^{14}N-^{14}N-^{17}O, and ^{14}N-^{14}N-^{18}O, where ^{15}N-^{14}N-^{16}O and ^{14}N-^{15}N-^{16}O are also referred to as 'isotopomers', or isotopic isotomers. The stable isotope ratios of nitrogen ($^{15}N/^{14}N$) and oxygen ($^{18}O/^{16}O$) in N_2O, are reported relative to standards atmospheric N_2 and VSMOW, respectively, using delta notation, where $\delta = (R_{N2O}/R_{std} -1)*1000$ (‰). The bulk values of $\delta^{15}N$ and $\delta^{18}O$ are affected by the substrate's isotopic composition and isotopic fractionation associated with chemical or enzymatic reaction. The isotope ratios thus serve as powerful tools to elucidate the N_2O cycling mechanisms, as each process imparts predictable isotopic fractionation on water column N_2O (Ostrom et al., 2007; Schmidt et al., 2004; Sutka et al., 2006; Toyoda, 2002; Toyoda et al., 2005). Due to the asymmetrical linear geometry of N_2O, the distribution of ^{15}N between isotopomers that contain ^{15}N in the inner (alpha: α) versus outer (beta: β) nitrogen atoms provide an independent constraint from the isotopes of N_2O beyond the bulk compositions of nitrogen and oxygen isotopes (Schmidt et al., 2004; Sutka et al., 2006; Toyoda et al., 2005; Toyoda & Yoshida, 1999). The difference in $\delta^{15}N$ of the inner and outer atoms in N_2O is known as site preference ($SP = \delta^{15}N^{\alpha} - \delta^{15}N^{\beta}$), and this value is thought to reflect the mechanism of N_2O production and consumption.

Through analysis of the isotopocules of N_2O, nitrate (NO_3^-), and nitrite (NO_2^-), in conjunction with supporting hydrographic and biogeochemical data, such as temperature, salinity, nutrient, and dissolved oxygen concentrations, we evaluated the mechanistic underpinnings of N_2O cycling in the ETSP during both ENSO states. Understanding the role ENSO has on N_2O cycling and emissions is imperative, as each ENSO event represents an altered climate-ocean dynamic that has occurred in the past or can occur in the future. To our knowledge, this work is the first to directly compare N_2O cycling under both phases of ENSO in the ETSP OMZ using isotopic measurements.

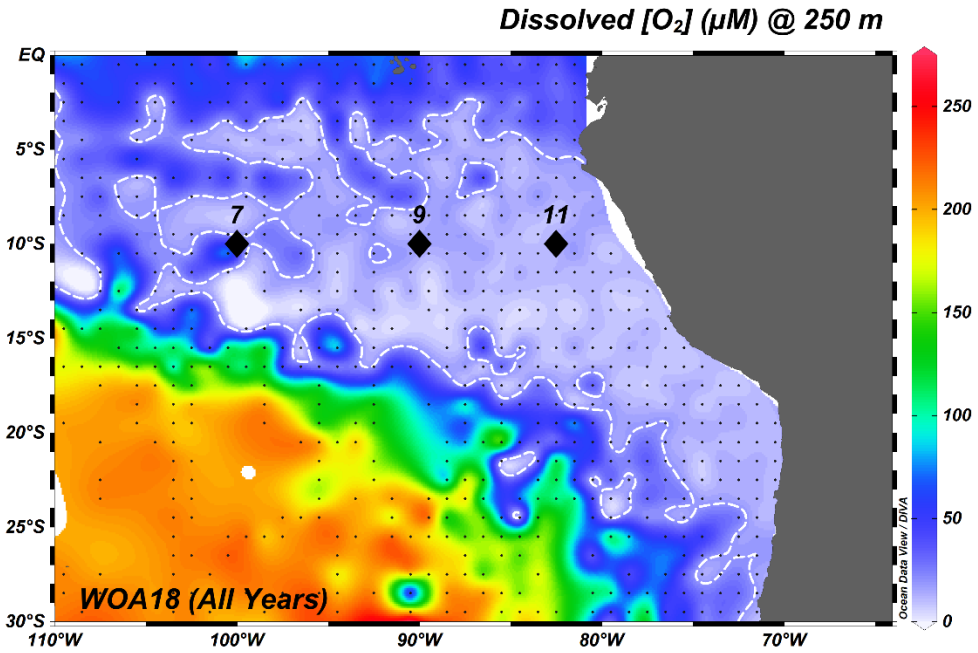

150

151 **Figure 1: Map of stations analyzed along 10 ºS (black diamonds): Station 7 (100 ºW), Station 9 (90 ºW), and**
152 **Station 11 (82.5 ºW) overlain on dissolved oxygen concentrations (µM) at 250 m from World Ocean Atlas**
153 **2018 (WOA18), using yearly averaged data from the entire climatology, illustrated using DIVA interpolation.**
154 **The limit of suboxic waters ($[O_2]$ < 20 µM) is illustrated in a dashed white contour line, and the locations of**
155 **grid points from WOA18 are shown in black dots.**

2. Materials and Methods

2.1 Cruise and N_2O Sampling Details

Samples for N_2O isotopes were collected from the ETSP OMZ aboard the R/V *Atlantis* (Cruise AT15-61) from January to March 2010 and R/V *Melville* (Cruise MV1104) from March and April 2011 (Knapp et al., 2016; Santoro et al., 2021). Three stations were evaluated for this work along 10 ºS: Station 7 (100 ºW), Station 9 (90 ºW), and Station 11 (82.5 ºW) (Fig. 1). Each cruise collected N_2O concentration and isotopocule samples at the same stations, with greater vertical sampling resolution during the 2011 cruise. The 2010 and 2011 cruises utilized a 24 and 36 Niskin bottle CTD rosette, respectively. N_2O samples were collected through silicone tubing directly into Wheaton 160 mL glass serum bottles (Wheaton prod. no. 223748) and overflowed twice before filling. The tubing was removed, and a 1 mL headspace was introduced into each bottle before capping with a grey butyl septum (MicroLiter Analytics Prod #20-0025). After collection, 100 µL of saturated mercuric chloride was added to each bottle and then resealed with the grey butyl septum and an aluminum crimp seal. Samples were stored in the dark at room temperature until analysis.

2.2 N_2O Isotopic Analysis

All 247 N_2O samples from the 2010 cruise were analyzed soon after the cruise at the Woods Hole Oceanographic Institution in 2010 using a Thermo Fisher Scientific Delta^{PLUS} XP isotope ratio mass spectrometer (IRMS) over approximately one month. Samples collected in the 2011 cruise were analyzed at Stanford University over three different analytical years and with two different instruments: a Delta^{PLUS} XP, used in 2012 and 2014, and a Thermo Fisher Scientific DeltaV Plus IRMS used in 2017. Of the 440 samples analyzed from the 2011 cruise, 324 (73.6%), 59 (13.4%), and 57 (13%) samples were analyzed in 2012, 2014, and 2017, respectively.

In all cases, samples were extracted and analyzed using a custom automated purge and trap inlet system and normalized to an injection of calibrated pure N_2O reference gas introduced prior to the elution of each sample peak (McIlvin & Casciotti, 2010). Isotope ratios were referenced initially to the calibrated N_2O reference tank to create a set of 'ratio of ratios' ($^{31}R_{sample}/^{31}R_{reference}$, $^{45}R_{sample}/^{45}R_{reference}$, $^{46}R_{sample}/^{46}R_{reference}$). Next, the data were size corrected in reference to a calibrated 20 volt-second (Vs) peak area for a mass to charge ratio of 44 (m/z 44). Finally, 'scrambling coefficients' were applied to the isotopomer data to correct the measured $^{15}R^{\alpha}$ and $^{15}R^{\beta}$ for the rearrangement of nitrogen atoms in N_2O when the gas is ionized in the mass spectrometer ion source (Frame et al., 2014; Frame & Casciotti, 2010; Kelly et al., 2021). The isotope ratios of N and O atoms in N_2O, $^{15}R_{sample}$ or $^{18}R_{sample}$, respectively, are expressed in delta notation (δ), where the $\delta^{15}N$ and $\delta^{18}O$ are defined relative to the isotope ratios of

certified standards: $\delta^{15}N$ or $\delta^{18}O = (R_{sample}/R_{standard} - 1)$ x1000. The $R_{standard}$ values used for $\delta^{15}N$ and $\delta^{18}O$ are the ratios of $^{15}N/^{14}N$ and $^{18}O/^{16}O$ in atmospheric N_2 and Vienna Standard Mean Ocean Water (VSMOW), respectively. Analytical precision for $\delta^{15}N^{\alpha}$, $\delta^{15}N^{\beta}$, SP, $\delta^{15}N^{bulk}$, and $\delta^{18}O$ for 2010 data were 0.33‰, 0.39‰, 0.66‰, 0.12‰, 0.2‰, respectively, and 1.25‰, 1.03‰, 2.08‰, 0.52‰, 0.89‰ for 2011 data, respectively.

Inconsistencies in the isotopocule data between the 2010 and 2011 datasets became apparent when data interpretation began. To assess isotopic offsets between the two cruise years, deep water samples (herein defined as all samples below 1000 m) for $\delta^{15}N^{bulk}$, SP, and $\delta^{18}O$ were evaluated. Samples from 2010 were plotted against those from 2011 found within five meters, and deviations from a 1:1 line were used to identify offsets. $\delta^{15}N^{bulk}$ values were higher in 2011 by approximately 1‰-2‰, except for three outliers that were about 3‰-5‰ below 2010 values, but the offset varied depending on the year the 2011 data were analyzed. SP had more variance in both directions from the 1:1 line, and $\delta^{18}O$ was consistently 2‰ higher in the 2011 samples than in 2010. Following the intercalibration methods used in (Mohn et al., 2014), we identified two potential methods for post-analysis corrections for N_2O isotopocules: an offset correction and a two-point correction. Ultimately, it was determined that an offset correction, using deep water isotopocule values as a comparative standard, would best serve our data correction needs. In this correction scheme, we averaged each isotopic value of N_2O for overlapping depths measured during the 2010 and 2011 cruises below 1000 m. We further broke the averages down for each analytical year for the 2011 measurements (2012, 2014, and 2017) and found the difference between each year's deep water isotopic values and the 2010 values. The difference was then applied as an offset to the 2011 cruise data to better resolve year to year differences in the N_2O isotopic measurements. The exact offset correction applied to the 2011 data can be found in the supplement (Table S1).

2.3 N_2O Concentrations

The N_2O concentration ($[N_2O]$) was also determined for each gas sample. The m/z 44 peak area for each sample was converted to a nmole quantity using a calibrated conversion factor between nmols of N_2O and peak area (Vs) of the mass 44 (McIlvin & Casciotti, 2010). Based on extraction system testing, the sample volume was assumed to be 153.8 ± 0.5 mL (McIlvin and Casciotti, 2010). Repeat measurements of duplicate N_2O samples yielded average $[N_2O]$ precisions for Stations 7, 9, and 11 of 0.54 nmol/L and 2.45 nmol/L for 2010 and 2011, respectively, and were previously reported (Santoro et al., 2021)

2.4 N_2O Air-Sea Flux

Air-sea N_2O flux calculations were performed for each station during both ENSO phases using measured average mixed layer [N_2O], the expected [N_2O] at equilibrium with the atmosphere, and the 10-meter wind speed (Wanninkhof, 2014). Calculations were made using monthly averaged 10-meter wind speed data for the month leading up to each station's sampling date. Wind speed was derived using the NCEP/NCAR Reanalysis 2 data product using four-time daily wind speed measurements and were averaged for the monthlong period (National Centers for Environmental Prediction, National Weather Service, NOAA, U.S. Department of Commerce, 2000). Atmospheric N_2O mixing ratios were derived from NOAA's Global Monitoring Laboratory (https://www.esrl.noaa.gov/gmd/hats/insitu/cats/conc.php?site=mlo&gas=n2o) and converted to equilibrium [N_2O] using the surface salinity and temperature data derived from the CTD (Weiss & Price, 1980). If atmospheric N_2O data were not available for the same day that the station was occupied, then the closest date of sampling was used.

2.5 Isotopic Analysis of Nitrate and Nitrite

All NO_3^- and NO_2^- isotopic analyses were performed using a Thermo Fisher Scientific Delta^{PLUS} XP IRMS. For sample preservation, NO_3^- and NO_2^- samples were filtered at sea, and NO_2^- isotopic samples were treated with 2 M sodium azide in 20% acetic acid in a crimp sealed 20 mL vial (McIlvin & Altabet, 2005). The NO_2^- sample preservation method, known as the "azide method," converts NO_2^- to N_2O which can then be analyzed on an IRMS (McIlvin & Altabet, 2005). During analysis, the produced N_2O was purged from the vial, cryogenically trapped, and analyzed on the IRMS. Samples were corrected against NO_2^- isotopic standards RSIL-N20, N7373, and N10219 made from sodium nitrite salts converted in parallel at sea (Casciotti et al., 2007). Nitrite isotope samples are reported in delta notation, where $\delta^{15}N\text{-}NO_2^-$ and $\delta^{18}O\text{-}NO_2^-$ are in reference to atmospheric N_2 and VSMOW, respectively. Precision for $\delta^{15}N\text{-}NO_2^-$ and $\delta^{18}O\text{-}NO_2^-$ in both 2010 and 2011 were approximately 0.2‰ and 0.3‰, respectively.

Nitrate isotope samples for $\delta^{15}N$ and $\delta^{18}O$ were analyzed in duplicates, at minimum, using the 'denitrifier method' which involves the microbial reduction of NO_3^- to N_2O (Casciotti et al., 2002; Sigman et al., 2001). These data are also reported in delta notation in reference to atmospheric N_2 and VSMOW, and samples were analyzed alongside reference material with known isotopic values (USGS32, USGS34, and USGS35). Samples were treated with sulfamic acid to remove NO_2^-, if present (Granger & Sigman, 2009). Analytical precisions for $\delta^{15}N\text{-}NO_3^-$ were 0.20‰ and 0.14 ‰ for 2010 and 2011, respectively, and precisions for 2010 and 2011 $\delta^{18}O\text{-}NO_3^-$ were 0.37‰ and 0.18‰, respectively.

2.6 El Niño-Southern Oscillation

The warm and cold phases of the El Niño-Southern Oscillation (ENSO), known as El Niño and La Niña, respectively, are defined through the National Oceanic and Atmospheric Administration (NOAA) Ocean Niño Index (https://origin.cpc.ncep.noaa.gov/products/analysis_monitoring/ensostuff/ONI_v5.php). ENSO events are determined when sea-surface temperature (SST) anomalies in the central equatorial Pacific region, known as Niño 3.4, are ± 0.5 ℃ over a 3-month running mean, using the previous 30 years as a baseline (NOAA's Climate Prediction Center, n.d.). Using the running mean of SST anomalies for the Niño 3.4 region for both cruise years, 2010 and 2011, they were defined as moderate El Niño and La Niña events, respectively.

3. Results

3.1 Study Site Characteristics

Stations 7, 9, and 11 during both cruise years maintained ODZ-like properties, such as having two N_2O maxima separated by a local minimum in N_2O concentrations, coinciding with the lowest dissolved O_2 concentrations (Fig. 2). These stations were also characterized by sustained suboxia ($[O_2] < 20$ μM) below the mixed layer into intermediate waters. Upwelling velocities, calculated using beryllium-7 (^7Be) measurements, were high at these stations (1.09-2.95 m d^{-1}) compared to other stations measured along 20 ºS (0-0.33 m d^{-1}) during the same expeditions, suggesting greater supply of "new" nutrients to the euphotic zone at 10 ºS (Berelson et al., 2015; Fuenzalida et al., 2009; Haskell et al., 2015).

The oxycline bases for Stations 9 and 11 were found at shallower depths during La Niña (75 m - 80 m) compared to El Nino (125 m - 200 m; Fig. 2). As a result, thicker ODZs were found during La Niña at Stations 9 and 11 compared to El Niño, and ODZ ventilation for all three stations occurred between 600 m and 700 m. At all stations during both years, a shallow N_2O concentration maximum was found at the base of the oxycline, with maximal oxycline N_2O concentrations ranging from 75 nM to 145 nM (Fig. 2). At Station 7, the most offshore station, a larger N_2O maximum was found in the oxycline during El Niño compared to La Niña despite having comparable oxycline depths during both ENSO states (Fig. 2A). However, the impacts of ENSO do not appear to have a substantive impact on the hydrographic features at Station 7, overall. At Stations 9 and 11, the $[N_2O]$ maximum at the base of the oxycline was larger, and shallower, during La Niña than during El Niño.

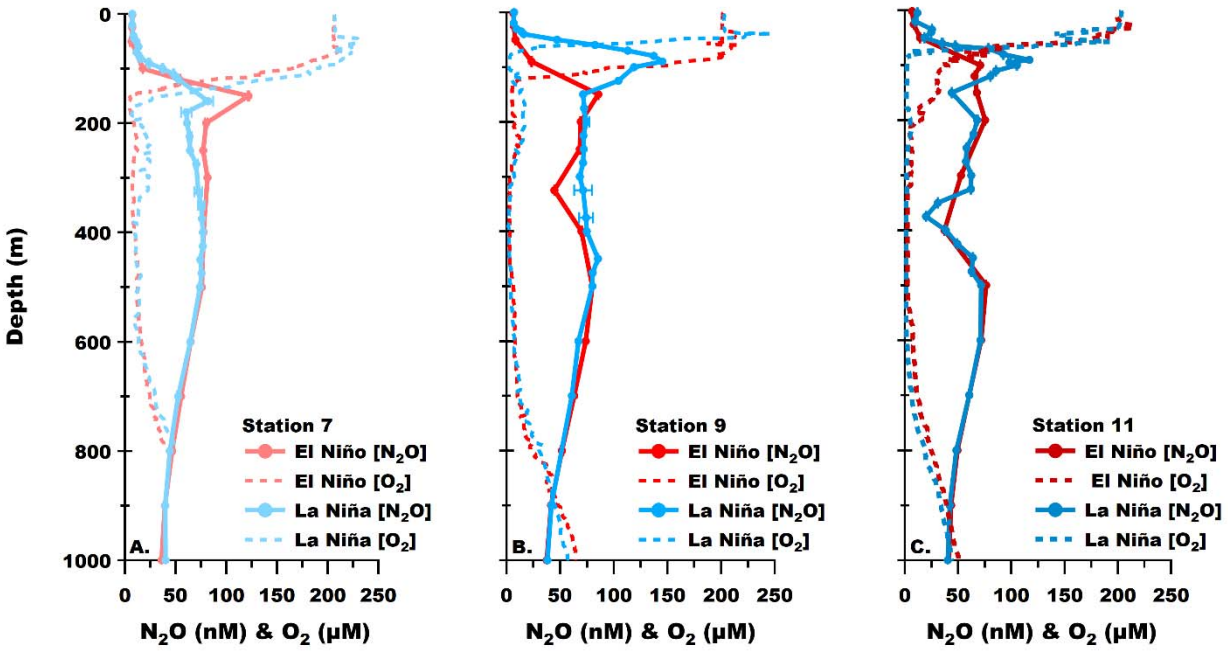

Figure 2: Dissolved N_2O (nmol/L; solid lines) and O_2 (µmol/L; dashed lines) concentrations for A) Station 7; B) Station 9; and C) Station 11. El Niño measurements are in shades of red, while La Niña measurements are in shades of blue.

A primary nitrite maximum (PNM) was observed at each station, ranging from 1 µM – 2 µM (Santoro et al., 2021). During El Niño, the PNM was found at greater depths moving westward, occurring at 40 m at Station 11 and 150 m at Station 7, with concentrations ranging from 1.2 µM - 1.4 µM. During La Niña, the PNM features were generally at lower potential density horizons and shallower depths, at 35 m-80 m depth, with concentrations ranging from 1 µM - 2 µM. A secondary nitrite maximum (SNM), indicative of functional anoxia, was found at Station 11 during both years, but only during El Niño at Station 9. At Station 11, the SNM reached 2.1 µM and 1.8 µM during El Niño and La Niña, respectively. A small, but measurable third nitrite peak of 0.5 µM was observed at Station 11 at 150 m during La Niña, where a sharp decrease in N_2O concentration was also measured. At Station 9 during El Niño, a SNM of 0.4 µM was observed at 325 m. Significant concentrations of ammonium between 1 µM-2.5 µM were also measured at all stations in both years, however, no ammonium measurements were made at Station 7 during El Niño (Santoro et al., 2021).

3.2 Upper Ocean N_2O Inventory and Atmospheric Flux

Apparent differences in the upper ocean N_2O inventory for Station 7, 9, and 11 led us to quantify the depth-integrated N_2O concentrations for comparison between stations and sampling campaigns (Fig. 3). Integrations were performed from 0 to 100 m at Stations 7, 9, and 11 using a trapezoidal Riemann sum. Because no measurement was made at 100 m at Station 9 during El Niño, we interpolated a value at 100 m between measurements made at 90 m and 150 m, to make comparable interpretations. N_2O accumulation was greater at every station during La Niña compared to El Niño, with Station 9 having a six-fold higher N_2O accumulation: from approximately 1 mmol/m^2 during El Niño to 5 mmol/m^2 during La Niña. While comparable in magnitude, N_2O accumulation at Station 11 was lower than Station 9, despite Station 11 being the closest station to the coast where N_2O cycling is presumably the most intense. Only a minor increase in N_2O accumulation was observed at Station 7 between El Niño and La Niña, as O_2 concentrations remained high during both years in the upper 100 m, thus limiting the difference in N_2O production between years.

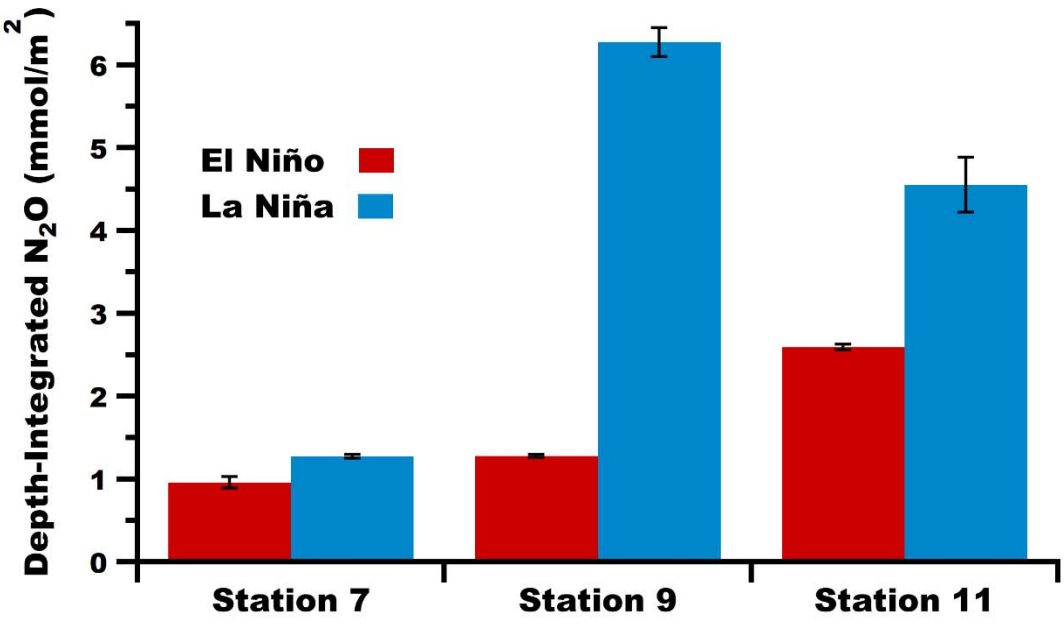

Figure 3: Depth-integrated N_2O during El Niño (red) and La Niña (blue) calculated to 100 m for Stations 7, 9, and 11.

Given comparable winds, higher N_2O accumulation in the upper 100 m and in the mixed layer should increase the N_2O flux to the atmosphere during La Niña relative to El Niño. Expanding on N_2O flux estimates from 2010 reported earlier (Santoro et al., 2021), estimated N_2O fluxes were up to two

orders of magnitude greater during La Niña than during El Niño (Table 1). Station 11 had the largest N_2O flux of 22.2 μmol m^{-2} d^{-1} during La Niña, which is primarily driven by the 173% saturation of [N_2O] at the surface.

Year	Station	Flux (μmol/m^2/d)
El Niño (2010)	7	1.5 (1.4-1.7)
	9	0.6 (0.5-0.6)
	11	4.3 (3.9-4.8)
La Niña (2011)	7	6.7 (6.1-7.5)
	9	6.5 (6.0-7.3)
	11	22.2 (20.3-24.8)

Table 1: Air-Sea fluxes of N_2O from all three stations during both ENSO phases. Surface N_2O concentrations for flux calculations were derived using the average mixed layer N_2O concentrations. Range of uncertainty given in parentheses is based on a 20% error associated with the Schmidt number.

3.3 $\delta^{15}N$ and $\delta^{18}O$ of Nitrite and Nitrate

During La Niña, trends of increasing $\delta^{15}N\text{-}NO_2^-$ and decreasing $\delta^{18}O\text{-}NO_2^-$ were observed from the surface into the oxycline at Station 9 (Fig. 4A). In contrast, NO_2^- isotopes at Station 11 during La Niña were relatively constant, ranging from -10.9‰ to -14.2‰ and 12.1‰ to 10.7‰ for $\delta^{15}N\text{-}NO_2^-$ and $\delta^{18}O\text{-}NO_2^-$, respectively (Fig. 4B). The one exception to this trend at Station 11 during La Niña was at 60 m where the $\delta^{15}N\text{-}NO_2^-$ increased to -3.2‰, which could be associated with enhanced nitrite reduction, or lower rates of nitrite oxidation. During El Niño, the lower nitrite concentrations and sampling resolution meant that only one measurement for $\delta^{15}N\text{-}NO_2^-$ and $\delta^{18}O\text{-}NO_2^-$ was made for each of Stations 9 and 11 in the upper 100 m (Fig. 4, S1). The $\delta^{18}O\text{-}NO_2^-$ measured during El Nino was similar to those values measured during La Nina, while $\delta^{15}N\text{-}NO_2^-$ was higher at Station 9 and lower at Station 11 (Fig. 4, S1).

The vertical distributions of $\delta^{15}N\text{-}NO_3^-$ and $\delta^{18}O\text{-}NO_3^-$ in the upper water column were impacted by ENSO in parallel with changes in chemical and physical properties, like the oxycline and density layers being found shallower in the water column during La Niña (Fig. 4, Fig. S1). Station 7 NO_3^- isotopes were similar between ENSO events, maintaining a surface maximum followed by a general decrease with depth (Fig. S2G). No changes were observed in $\delta^{15}N\text{-}NO_3^-$ or $\delta^{18}O\text{-}NO_3^-$ at ODZ depths at Station 7, which is consistent with the lack of variation in N_2O concentration and isotopes between ENSO phases at this station. At Stations 9 and 11, high surface $\delta^{15}N\text{-}NO_3^-$ and $\delta^{18}O\text{-}NO_3^-$ were found during both ENSO events, however, the decrease in $\delta^{15}N\text{-}NO_3^-$ and $\delta^{18}O\text{-}NO_3^-$ occurred at shallower depths and followed a

steeper gradient during La Niña (Fig. 4B, C). In fact, the shallow NO_3^- isotope minimum was measured 90 m shallower at Station 9 during La Niña compared to El Niño (Fig. 4B). Both $\delta^{15}N\text{-}NO_3^-$ and $\delta^{18}O\text{-}NO_3^-$ were elevated within the ODZ at Stations 9 and 11 during El Niño, consistent with nitrate reduction occurring within the ODZ. A similar level of heavy isotope enrichment was observed during La Niña at Station 11, but less so at Station 9. The depths where elevated $\delta^{15}N\text{-}NO_3^-$ and $\delta^{18}O\text{-}NO_3^-$ values were found corresponded with the lowest [N_2O] in the ODZs, supporting the impact of denitrification on water column N species distributions. Though the nitrate isotope profiles shoaled during La Niña, $\delta^{15}N\text{-}NO_3^-$ and $\delta^{18}O\text{-}NO_3^-$ appear to be significantly less sensitive to the contrasting biogeochemical impacts imparted by each ENSO state, relative to N_2O.

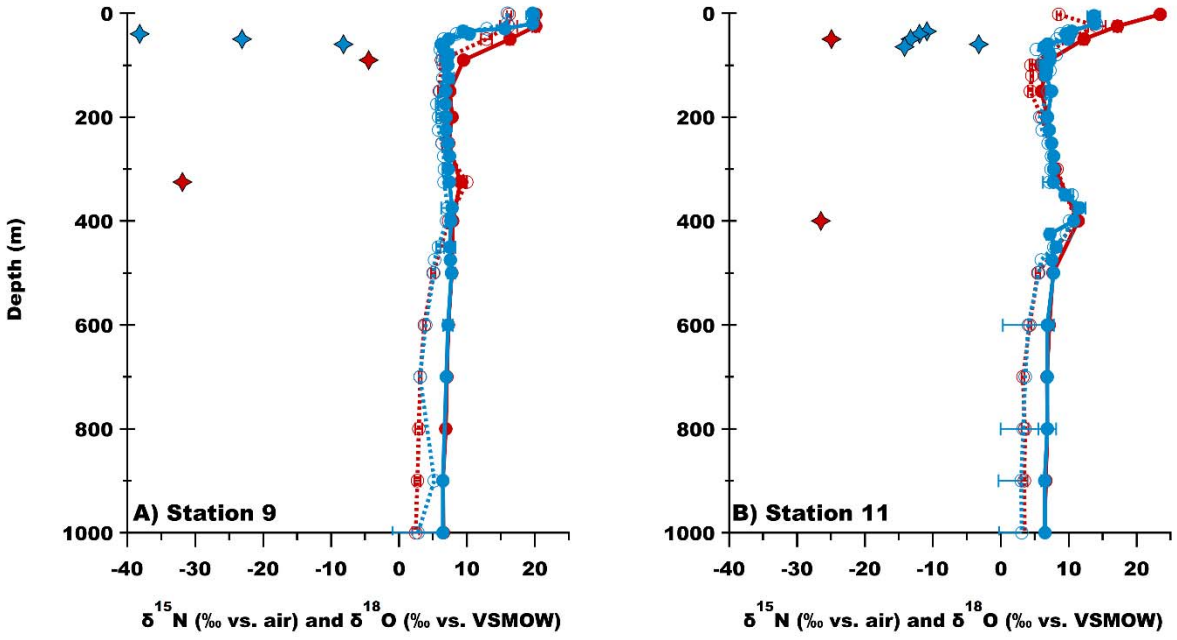

Figure 4: Station 9 (A) and Station 11 (B) $\delta^{15}N\text{-}NO_3^-$ (filled circles, solid line), $\delta^{18}O\text{-}NO_3^-$ (open circles, dashed line), and $\delta^{15}N\text{-}NO_2^-$ (diamonds). Data from El Niño (red) and La Niña (blue).

3.4 Isotopic Composition of N_2O

At each station in both years, surface $\delta^{15}N^{bulk}$, closely reflected the isotopic composition of atmospheric N_2O, ranging from 5.8 - 6.8‰ (Fig. 5B). $\delta^{15}N^{bulk}$ generally decreased to subsurface minima, ranging from 2.8‰ to 5‰, coinciding with the near surface [N_2O] maxima. For Stations 9 and 11, distinct increases in $\delta^{15}N^{bulk}$ were observed from the shallow $\delta^{15}N^{bulk}$ minimum to their ODZ maxima, found between 325 - 400 m (Fig. 5). Conversely, the increase in $\delta^{15}N^{bulk}$ at Station 7 was more gradual and did not exhibit a defined peak in the ODZ (Fig. S2B). A unique shallow $\delta^{15}N^{bulk}$ maximum was found at 150 m at Station 11 during La Niña, corresponding to increases in other isotopocule measurements and a

decrease in N_2O concentration. This feature is sandwiched between two lower $\delta^{15}N^{bulk}$ values and larger N_2O concentration measurements, thus, potentially reflecting intrusion of anoxic waters that had experienced N_2O consumption.

Similar to $\delta^{15}N^{bulk}$, mean $\delta^{18}O$-N_2O values in surface waters generally reflected that of atmospheric N_2O, averaging 45.5‰ in both years (Fig. 5C). At all stations during El Niño, and Station 7 during La Niña, $\delta^{18}O$-N_2O slightly decreased from the surface to 40-43‰ near 100 m, then gradually increased to maximum values of 55-80‰ in the ODZ, where [N_2O] decreased (Fig. S2, S3). During La Niña, $\delta^{18}O$-N_2O initially decreased to a minimum at 50 m at Station 9 and then increased to 48.6‰ at 100 m, below the [N_2O] maximum at 90 m. Station 11 during La Niña demonstrated the most variability in the upper 100 m, and it had the largest observed $\delta^{18}O$-N_2O of 94‰ in the ODZ (Fig. S3). Also at Station 11 during La Niña, a significant near surface $\delta^{18}O$-N_2O peak of 79.5‰ at 150 m coincided with the reduction in N_2O concentration and elevated $\delta^{15}N^{bulk}$ mentioned above.

The distribution of $\delta^{15}N^{\alpha}$ in both years was tightly coupled to the distribution of $\delta^{15}N^{bulk}$ and $\delta^{18}O$-N_2O (Fig. 5E). During both years, $\delta^{15}N^{\alpha}$ values decreased from near-surface values to minima (6-9.5‰) in the oxycline, above the [N_2O] maximum. Local maxima in $\delta^{15}N^{\alpha}$ occurred at 90 m at Station 9 and 150 m at Station 11 during La Niña. Subsurface $\delta^{15}N^{\alpha}$ maxima (17.3-31.6‰) coincided with water column [N_2O] minima in the anoxic core of the ODZ at Station 11 (Fig. 5). These $\delta^{15}N^{\alpha}$ maxima also coincided with elevated $\delta^{18}O$-N_2O and $\delta^{15}N^{bulk}$, likely representing N_2O consumption.

Surface values of $\delta^{15}N^{\beta}$ were typically low, ranging between -4.5‰ and -1‰, which span the expected atmospheric value of -3.3‰. From there, $\delta^{15}N^{\beta}$ decreased into the [N_2O] maxima at Stations 9 and 11 during La Niña, whereas $\delta^{15}N^{\beta}$ values slightly increased at the [N_2O] maximum during El Niño. The minima in $\delta^{15}N^{\beta}$ seen at Stations 9 and 11 corresponded with lower $\delta^{15}N^{bulk}$ and higher $\delta^{18}O$-N_2O values in the upper 100 m (Fig. 5, S3). Low $\delta^{15}N^{\beta}$ values are often observed within oxygen deficient waters. Indeed, the $\delta^{15}N^{\beta}$ values reached their overall minima with the ODZ coinciding with marked decreases of [N_2O] in both ENSO phases at Station 11. Thus, the $\delta^{15}N^{\beta}$ minima found in oxycline waters at Stations 9 and 11 during La Niña (where high N_2O accumulation was measured) may result from a different set of processes that will be further addressed below (Fig. S3).

Site preference (SP) values in surface waters ranged from approximately 13.8 - 21.4‰, which span the atmospheric value of 19‰ (Mohn et al., 2014). A subsurface SP minimum found near the base of the oxycline at each station ranged from 5.5 - 9.2‰, with the lowest SP observed in the oxycline at Station 11 during La Niña. During La Niña, high SP values (20 - 44‰) were found at 150 m and within the ODZ, coinciding with marked reductions in N_2O concentrations, as well as elevated $\delta^{18}O$-N_2O and

391 $\delta^{15}N^{bulk}$ values (Fig. S3). At Station 9 in La Niña, however, the SP maximum at 90 m coincided with the
392 station's near-surface N_2O concentration maximum and corresponded with a local maximum in $\delta^{15}N^{\alpha}$ and
393 minimum in $\delta^{15}N^{\beta}$ (Fig. 5E & 5F).

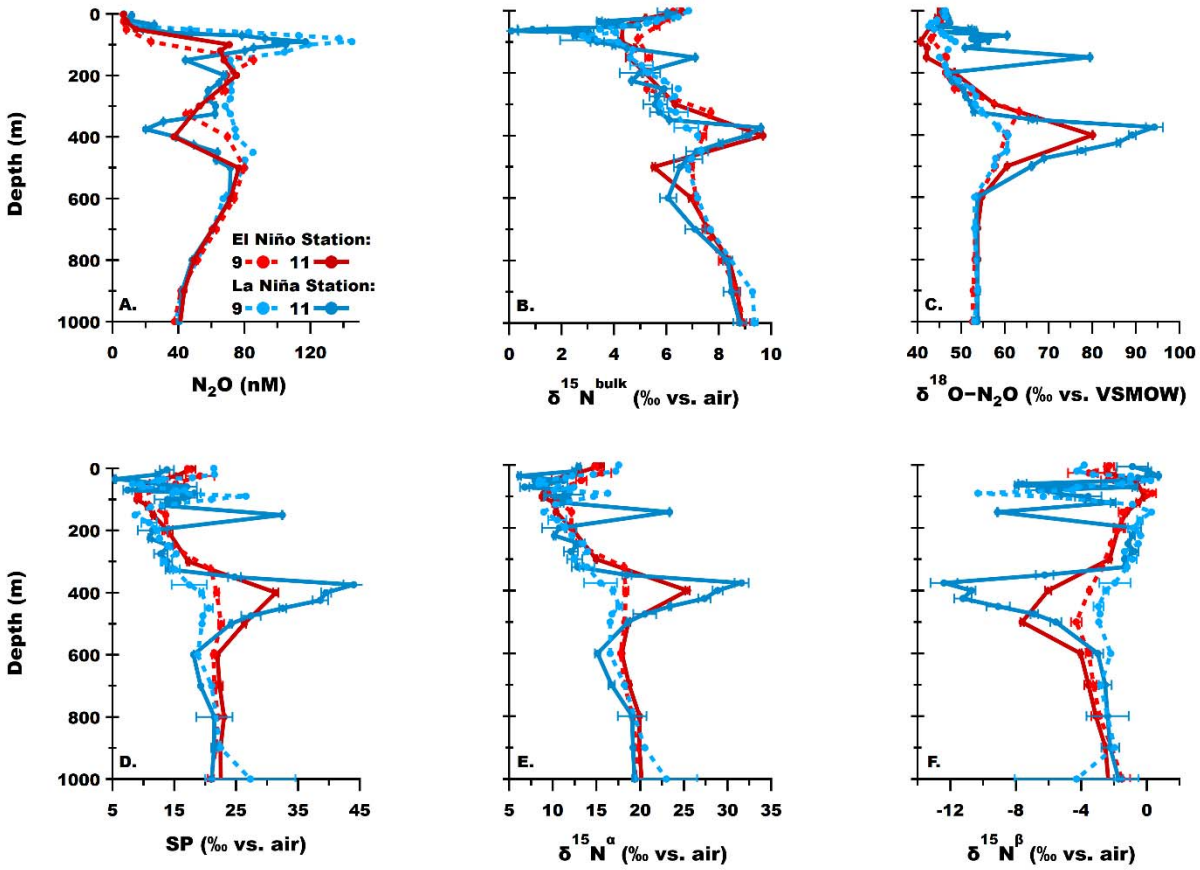

394

395 **Figure 5: N_2O A) concentrations (nM); B) $\delta^{15}N^{bulk}$ (‰ vs. air); C) $\delta^{18}O$ (‰ vs. VSMOW); D) SP (‰ vs. air);**
396 **E) $\delta^{15}N^{\alpha}$ (‰ vs. air); and F) $\delta^{15}N^{\beta}$ (‰ vs. air) illustrated for Stations 9 (90 ºW; dashed line) and 11 (82.5 ºW;**
397 **solid line) during El Niño (red) and La Niña (blue).**

398 ## 4. Discussion

399 ### 4.1 La Niña Shoaling Increased N_2O Flux and Accumulation

400 Our data demonstrated a 100-fold increase in the estimated N_2O flux to the atmosphere (Table 1)
401 and up to a six-fold increase in accumulated N_2O in the upper 100 m of the water column between El
402 Niño and La Niña (Fig. 3), as major biogeochemical features like the N_2O maximum corresponding with
403 the oxycline base were shoaled into this layer (Fig. 2). During El Niño, the trade winds weakened,
404 resulting in the return of warm, salty surface waters to the eastern Pacific, a deepening of the mixed layer,
405 and slowed coastal upwelling. The opposite occurred during La Niña, where enhanced upwelling

transported sub-surface N_2O into shallower depths. Similarly, N_2O at shallower depths were likely upwelled into the mixed layer leading to the increase in N_2O fluxes during La Niña. Atmospheric backtracking demonstrated a significantly greater N_2O flux in our study region during La Niña compared to El Niño (Babbin et al., 2020); our results provide a complementary ocean-based view of these findings. Whether the larger accumulation of N_2O in the upper 100 m during La Niña is due to transport alone or also due to alterations to the pathways of N_2O formation are evaluated below.

4.2 Limited N_2O Cycling in Surface and Oxycline Waters During El Niño

Although limited by lower sample resolution, little isotopocule heterogeneity was observed above the oxyclines at Stations 9 and 11 during La Niña, as well as in and above the Station 9 and 11 oxyclines during El Niño (Fig. 5). In these regions, similar isotopocule values and trends indicate similar sources with low N_2O production rates due to the low N_2O accumulation. Generally, N_2O in these waters had lower $\delta^{18}O\text{-}N_2O$, SP, and $\delta^{15}N^{\alpha}$ values relative to atmospheric N_2O with increasing depth, while $\delta^{15}N^{\beta}$ increased. These same isotopocules in the El Niño oxyclines of Stations 9 and 11 corresponded with lower N_2O accumulation relative to La Niña. The moderate SP (9.1‰-17.1‰; Fig. 5D) and low $\delta^{18}O\text{-}N_2O$ (Fig. 5C) observed in the El Niño oxyclines does not point to a single specific N_2O source. While prior studies have shown N_2O production rates from NH_4^+ reached maximum values in the upper oxycline at Stations 9 and 11 during El Niño, indicating a role for hybrid N_2O production, rates of hybrid n2o production can be up to 2 orders of magnitude lower than incomplete denitrification (Ji et al., 2015; Santoro et al., 2021). It is also possible that lateral mixing from more coastal waters -- where incomplete denitrification can produce N_2O with a low SP -- is influencing the isotopic composition of N_2O we observed in the oxyclines of Stations 9 and 11 during El Niño, as described in other work (Fig. 6; Ji et al., 2019). Finally, due to the significant deepening of the thermocline that occurs during El Niño, it is likely that local production of N_2O was diminished in the less steep oxycline during this time. Under these conditions, consumption of NH_4^+ or organic matter would be concentrated in the upper oxycline waters where O_2 concentrations are still high enough to maintain low N_2O yields from ammonia oxidation. Thus, the combination of low N_2O accumulation and low isotopic heterogeneity in El Niño surface and oxycline waters and La Niña surface waters suggest limited local cycling of N_2O.

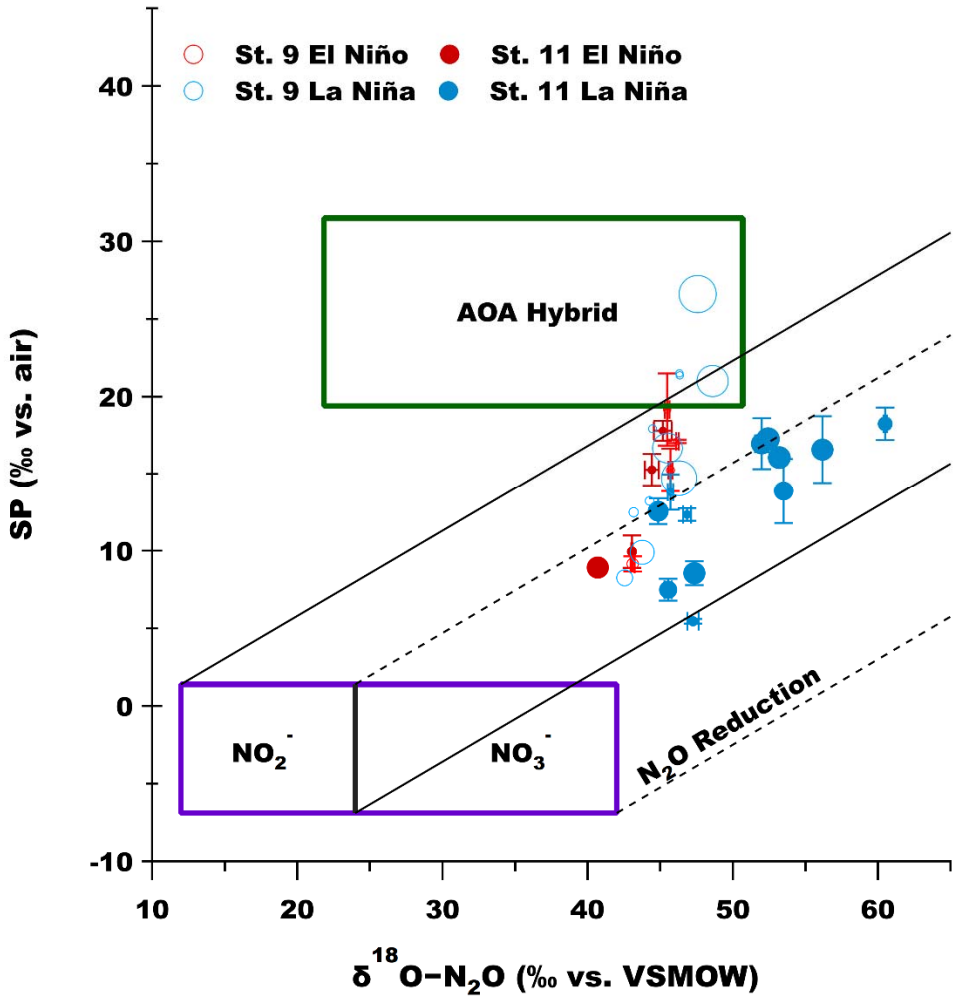

433

434 **Figure 6. N_2O Isotope mixing plot for $\delta^{18}O$ vs SP. Stations 9 and 11 samples from both ENSO states**
435 **in the upper 100 m are illustrated. Marker sizes indicates N_2O concentration in nM ranging from**
436 **6.6 nM to 145.2 nM. Range of potential delta values for N_2O produced by AOA hybrid production**
437 **(green box) and incomplete denitrification from NO_2^- (left purple box) or NO_3^- (right purple box)**
438 **are shown. Known regression slopes for N_2O consumption from nitrite (black solid lines) and**
439 **nitrate (dashed solid lines) are also illustrated.**

440 **4.3 Intense N_2O Cycling Through Multiple Pathways in Oxycline Waters During La Niña**

441 We used our measured N_2O, NO_2^-, and NO_3^- isotopic data data together with previously published
442 SP values to examine the potential relative contributions of competing microbial N_2O production and
443 consumption pathways (Fig. 6). The high accumulation of N_2O in the oxyclines of Stations 9 and 11
444 during La Niña demonstrated distinct isotopic values that point toward local production from incomplete
445 denitrification with overprinting signals of hybrid production and/or N_2O consumption (Fig. 6). During

La Niña at Station 9, from the top of the oxycline at 50 m to the [N_2O] maximum at 90 m, increases in SP and $\delta^{18}O$-N_2O coincided with a decrease in $\delta^{15}N^{\beta}$ (Fig. 5C, D, F). Additionally, from 50 m to 60 m, the $\delta^{15}N$ of NO_2^- significantly increased from -23.12‰ to -8.16‰, corresponding with the N_2O-$\delta^{15}N^{\beta}$ minimum found 5 m below (-7.9‰; Fig. 5B). The increased $\delta^{15}N$-NO_2^- indicates that NO_2^- reduction likely superseded NO_2^- oxidation there, as NO_2^- reduction causes ^{15}N enrichment in NO_2^- (Martin & Casciotti, 2016), whereas NO_2^- oxidation exhibits an inverse isotope effect (Casciotti, 2009), thus supporting a role for enhanced N_2O production from NO_2^-. At the same time, the SP values exceed that expected from incomplete denitrification, and suggest a role for an additional source from hybrid N_2O production (Fig. 6). Indeed, most of the points from the Station 9 La Nina oxycline fall within the mixing space between the hybrid pathway and denitrification of NO_3^-, or solely within the isotopic composition expected from hybrid N_2O production (Fig. 6). Recent modeling studies suggest that overall denitrification increases during La Niña in the ETSP due to a shoaling and expansion of low O_2 waters (Mogollón & Calil, 2017; Yang et al., 2017). Together, these effects could allow denitrifying organisms to utilize organic matter closer to the surface, where there is a greater organic matter flux, resulting in more production and consumption of N_2O via denitrification, thus corroborating our findings in our study.

Station 11 during La Niña exhibited signals of N_2O production from hybrid N_2O production and incomplete denitrification with evidence of partial N_2O consumption (Fig. 6). Consistently lower $\delta^{15}N^{bulk}$ (Fig. 5B) and increased $\delta^{18}O$-N_2O values (Fig. 5C) between the surface and the [N_2O] maximum of Station 11 during La Niña reflect a low substrate $\delta^{15}N$ and significant enrichment of ^{18}O in N_2O, respectively, two indications for N_2O production from the denitrification of NO_2^- or co-occurring production and consumption (Bourbonnais et al., 2017; Casciotti et al., 2018). The higher $\delta^{18}O$-N_2O values measured at Station 11, compared to Station 9, during La Niña could represent: 1) a greater contribution of N_2O from NO_3^- relative to NO_2^- due to its larger branching isotope effects; 2) a small, but significant overprinting signal of N_2O consumption, or 3) a combination of these effects.

Most data from Station 11 during La Niña extend from between the nitrate and nitrite bounds or as a mixture of hybrid and incomplete denitrification, suggesting a potential combination of N_2O substrates and sources (Fig. 6). In particular, the low $\delta^{15}N^{\beta}$ and $\delta^{15}N^{bulk}$ values paired with the most elevated $\delta^{18}O$-N_2O point toward incomplete denitrification as a significant production mechanism. Specifically, the low $\delta^{15}N^{bulk}$ and $\delta^{15}N^{\beta}$ values in the oxycline could represent NO_2^- as a key source of N_2O due to the low $\delta^{15}N$-NO_2^- values measured. The $\delta^{15}N$-NO_2^- values in the oxycline during La Niña ranged from -38.2‰ to -8.16‰ and -14.18‰ to -3.22‰ at Stations 9 and 11, respectively (Fig. 4A, B), thus representing an ^{15}N-depleted pool that would decrease $\delta^{15}N^{bulk}$ and $\delta^{15}N^{\beta}$ values in N_2O. In contrast, $\delta^{15}N$-NO_3^- values ranged from 5-20‰ over this depth range (Fig. 4). The cluster of Station 11 La Niña

data outside of the mixing bounds of the potential source boxes with $\delta^{18}O\text{-}N_2O > 50‰$ are unique to this station (Fig. 6). The enhancement of both $\delta^{18}O\text{-}N_2O$ and SP for these data likely results from N_2O consumption occurring on top of the background N_2O source mixture, whereas Station 9 data points during La Niña are found within the mixing bounds of hybrid production and incomplete denitrification sources.

In addition to denitrification, hybrid N_2O production likely also contributed to the accumulation of N_2O at Station 11 during La Niña (Fig. 6). In prior work, a relatively high rate of N_2O production from NH_4^+ was measured at 70 m in the Station 11 oxycline during La Niña (0.156 nmol N L^{-1} d^{-1}; Santoro et al., 2021). Additionally, Station 11 in La Niña corresponded with the highest abundance of Water Column A ammonia monooxygenase genes (*amoA*), a genetic marker for AOA (Santoro et al., 2021). Thus, the easternmost station, where we observed the greatest variability of N_2O cycling in oxycline waters, also has a high potential for ammonia oxidation to N_2O due to an abundant AOA community.

While mixing between N_2O production from the hybrid mechanism and incomplete denitrification can partially explain the increase in SP (and $\delta^{18}O\text{-}N_2O$) in the oxycline waters of Stations 9 and 11, modeling work has also suggested that denitrification with a positive SP (25‰), which has been shown to occur for one strain of denitrifying bacteria (Toyoda et al., 2005), may play an important role in N_2O dynamics in ODZ regions (Casciotti et al., 2018; Kelly et al., 2021; Monreal et al., 2022). In this case, denitrification could itself explain the isotopic patterns. Alternatively, hybrid N_2O production by AOA could produce N_2O with a SP that is lower than 30‰. For example, AOA from soils were shown to produce N_2O with SP ranging from 20‰-30‰ (Jung et al., 2014). Although the enzymology and exact mechanism of this reaction have yet to be described, its hybrid nature implies that it could have a variable SP. This is because the $\delta^{15}N$ difference between the alpha and beta nitrogen positions could be affected by independent variations in the oxidized and reduced substates combining to form hybrid N_2O. Thus, the production of N_2O via incomplete denitrification with a site preference, or hybrid N_2O production with a lower SP, cannot be excluded from consideration in the interpretation of N_2O isotopocule analysis in low O_2 waters. If this is the case, they could provide an explanation for the high measured SP values coinciding with elevated $\delta^{18}O\text{-}N_2O$ and low $\delta^{15}N^{\beta}$ and $\delta^{15}N^{bulk}$ values found here. Finally, culture experiments have also demonstrated the ability for fungi produce to N_2O with a high SP of ~22-37‰ through a 'denitrification-like' pathway (Maeda et al., 2015; Rohe et al., 2014; Sutka et al., 2008). Indeed, fungi have been observed to account for as much as 50% of the total N_2O produced at certain depths in the low oxygen waters of the ETSP, thus representing a significant source of N_2O and potential driver for non-traditional expectations of N_2O isotopomers (Peng & Valentine, 2021).

4.4 The Dynamic Nature of N_2O at Station 11 during La Niña

We expanded on the results of the mixing diagram (Fig. 6) and applied an open and closed system irreversible kinetic Rayleigh model to determine what fraction of N_2O needed to be consumed via denitrification to explain the elevated SP and $\delta^{18}O$ values at Station 11 during La Niña. There, data points in the isotope mixing diagram were found outside of the source mixing bounds and must have incurred N_2O consumption (Fig. 6). The open system Rayleigh model (Eq. 2) assumes steady state, meaning that the N_2O we observed would be explained by the continuous balance of production and consumption signals. Alternatively, the closed system Rayeligh model (Eq. 3) assumes non-steady state whereby a parcel of N_2O is being consumed without replenishment.

$$\delta_{obs} = \delta_{predicted} + \varepsilon * [1 - f] \quad (2)$$

$$\delta_{obs} = \delta_{predicted} - \varepsilon * \ln(f) \quad (3)$$

We used measured isotopocule values within the source mixing bounds and values found outside of the source mixing bounds as our $\delta_{predicted}$ and $\delta_{observed}$ values, respectively. Depending on whether we used the $\delta^{18}O$-N_2O or SP as our isotopocule values in the models and their associated isotope effects for N_2O consumption (ε), we calculated between 50-60% of the N_2O remained (*f*) after consumption using the closed system model and 30-50% of the N_2O remained after consumption using the open system model. Thus, given the cluster of Station 11 La Niña measurements found outside of the source mixing bounds with strongly negative $\delta^{15}N^{\beta}$ values, co-occurring production and consumption of N_2O must be occurring there to explain the N_2O isotopic composition. While the results of both Rayleigh model scenarios are plausible, modelling work has shown that ODZ environments may not be in steady-state, and thus, the results of closed system model may be more representative of the amount of N_2O consumption that has occurred at Station 11 during La Niña.

Parallel measurements on these cruises indicate non-steady state hydrographic conditions at Station 11 in 2011, during La Niña, which could explain the nature of N_2O concentrations and isotopocules measured there. For example, ^{7}Be measurements were found to exceed the expected value for water below the mixed layer, and upwelling velocities were up to an order of magnitude higher than all other stations during La Niña, thus representing the potential for substantial bidirectional vertical movement (Haskell et al., 2013) (Haskell et al., 2015). Additional work from these cruises similarly found high variability for ^{234}Th measurements in the upper 100 m at Station 11 during La Niña, also indicating non-steady state conditions. The "zig-zagging" nature of our N_2O isotopic profiles, such as $\delta^{18}O$-N_2O, at Station 11 during La Niña loosely mimics the variability observed in the ^{234}Th measurements found in Haskell 2013, potentially representing similar physical mechanisms.

We suggest that the variable N_2O isotopic content found at Station 11 during La Niña also represents non-steady state conditions, whereby ODZ waters in which N_2O consumption via denitrification has occurred have mixed into the oxycline. The notion that low-oxygen waters with partial N_2O consumption may be interacting with more oxic waters during La Niña is not surprising due to the higher predicted rates of denitrification and generally greater kinetic energy and stronger upwelling velocities found during La Niña, which can respond rapidly depending on local fluctuations in wind patterns (Mogollón & Calil, 2017).

4.5 The Isotopic Composition of Accumulated N_2O

To better describe the impacts ENSO has on the sources of N_2O in the upper 100 m of the water column, we calculated a depth-averaged isotope value (δ_{avg}) for the accumulated N_2O at each station:

$$\delta_{avg} = \frac{\sum_{i=1}^{n}\left[\left(\frac{\delta_i \times [N_2O]_i + \delta_{i-1} \times [N_2O]_{i-1}}{2}\right) \times (z_i - z_{i-1})\right]}{\sum_{i=1}^{n}\left[\left(\frac{[N_2O]_i + [N_2O]_{i-1}}{2}\right) \times (z_i - z_{i-1})\right]} \quad (1)$$

where δ_i is the isotopic composition of N_2O measured for sample i at depth z_i, and $[N_2O]_i$ is the N_2O concentration at that depth. The sum of these concentration-weighted isotopic values is then divided by the depth-integrated N_2O concentration for the depth range under consideration (Table 2).

We initially applied a Keeling model, a commonly used isotope and mass balance equation, to compute the isotopic composition of the produced N_2O from these data (Casciotti et al., 2018; Fujii et al., 2013; Yamagishi et al., 2007); however, there were evident violations of the model's assumptions, such as N_2O consumption. Comparing differences in the depth-averaged N_2O isotopic composition provides a holistic view of the net changes in accumulated N_2O in the upper 100 m between El Niño and La Niña conditions. As expected from inspection of the depth profiles (Fig. S2), the depth-averaged isotope calculations at Station 7 showed no substantive changes between El Niño and La Niña (Table 2). As described in Section 4.2, low N_2O accumulation coupled with low variability in the isotopocule measurements suggest little change in the rates and mechanisms of N_2O production at Station 7 between ENSO states. Here at Station 7, we rule out significant inputs from local denitrification as oxygen concentrations are most likely too high to support reductive processes. However, the isotopocule signals could be explained by a mixture of hybrid N_2O production and N_2O derived from denitrification, via long-range transport.

El Niño	$\delta^{15}N^{\alpha}_{avg}$	$\delta^{15}N^{\beta}_{avg}$	SP_{avg}	$\delta^{15}N^{bulk}_{avg}$	$\delta^{18}O_{avg}$-N_2O
Station 7	13.2 (0.1)	-1.6 (0.1)	14.8 (0.2)	5.8	45.4 (0.1)
Station 9	11.5 (0.2)	-0.9 (0.3)	12.4 (0.5)	5.3 (0)	44.2 (0.1)

Station 11	9.4 (0.1)	-0.5 (0.1)	9.9 (0.2)	4.5 (0)	41.6 (0.1)
La Niña	$\delta^{15}N^{\alpha}_{avg}$	$\delta^{15}N^{\beta}_{avg}$	SP_{avg}	$\delta^{15}N^{bulk}_{avg}$	$\delta^{18}O_{avg}$-N_2O
Station 7	12.5 (1.1)	-0.9 (0.8)	13.4 (1.9)	5.8	44.1 (0.4)
Station 9	12.3 (1.2)	-5.2 (1.0)	17.5 (2.3)	3.6 (0.2)	46.0 (0.2)
Station 11	10.1 (0.7)	-4.1 (0.4)	14.2 (1.1)	3.0 (0.3)	51.9 (0.2)

Table 2: Depth-averaged N_2O isotopocule values (in ‰) for the upper 100 m. Clear increases in $\delta^{18}O_{avg}$-N_2O and SP_{avg} and decreases in $\delta^{15}N^{bulk}_{avg}$ and $\delta^{15}N^{\beta}_{avg}$ occurred at Stations 9 and 11 from El Niño to La Niña, whereas, only minute changes were calculated at Station 7. Calculation uncertainties (in parantheses) were based on the standard deviation of each isotopic measurement, instead of the calculated δ_{avg}-values from Equation 1.

At Station 9, the depth-averaged $\delta^{15}N^{\beta}$ and $\delta^{15}N^{bulk}$ during La Niña were lower by 4.3‰ and 1.7‰, respectively, compared to El Niño. However, no significant change to $\delta^{15}N^{\alpha}$ was observed. To achieve this, a source relatively depleted in ^{15}N must be contributing to $\delta^{15}N^{\beta}$ during La Niña, while a competing mechanism maintains a steady $\delta^{15}N^{\alpha}$. At the same time, there was a six-fold increase in the overall N_2O accumulation during La Niña from the previous year's El Niño, thus N_2O production is likely enhanced by the significantly steeper and shallower oxycline found during La Niña (Fig. 7). From this, we again propose N_2O production from mixed sources with the potential for NO_2^- to be an important substrate of N_2O in these waters to lower the $\delta^{15}N^{\beta}$ during La Niña, while hybrid production from AOA or partial N_2O consumption could be maintaining the $\delta^{15}N^{\alpha}$ values. The combined effect of these processes on the isotopic composition of N_2O could support the intermediate SP and $\delta^{18}O$-N_2O values found during La Niña where N_2O accumulation was enhanced (Fig. 6). The low N_2O accumulations found at Station 9 during El Niño, as well as its isotopocule signatures, appeared to be similar to Station 7, reflecting relatively low N_2O production in the upper 100 m.

The largest apparent difference in N_2O sources between ENSO phases occurred at Station 11. The depth-averaged $\delta^{18}O$-N_2O during La Niña was 10‰ greater than during El Niño, indicating a greater role for N_2O production and/or consumption from denitrification during La Niña. Similar to Station 9, $\delta^{15}N^{\beta}$ and $\delta^{15}N^{bulk}$ values were 3.6‰ and 1.4‰ lower, respectively, during La Niña. Despite the high N_2O concentrations, we believe that the higher $\delta^{18}O$-N_2O values observed during La Niña reflect co-occurring N_2O consumption overprinting strong production signals at Station 11 (Fig. 6). For example, at 80 m during La Niña, we observed increases in $\delta^{18}O$-N_2O and SP concurrent with a decrease in $\delta^{15}N^{\beta}$, which could be indicative of simultaneous N_2O production and consumption in suboxic waters ($[O_2]$ = 7.2 µM) (Fig. 5; Bourbonnais et al., 2017; Casciotti et al., 2018). These conditions contrast with the upper 100 m

598 during El Niño, in which [O_2] reached a minimum of ~38 µM. During El Niño, the calculated SP (9.84‰)
599 and δ^{18}O-N_2O (41.38‰) achieved the lowest values observed for all stations in either ENSO event (Fig.
600 S2C, D). Consequently, we suggest that hybrid N_2O formation and a lesser degree of N_2O consumption
601 via denitrification resulted in the depth-averaged SP and δ^{18}O-N_2O values we found during El Niño
602 (Bourbonnais et al., 2017; Casciotti et al., 2018; Ji et al., 2019).

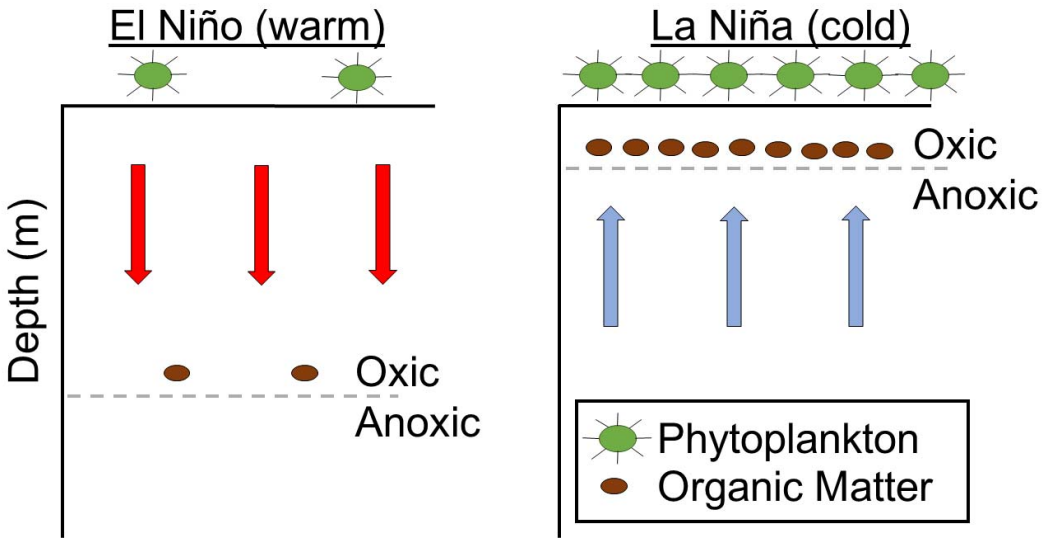

603

604 **Figure 7: Idealized cartoon highlighting key hydrographic and biogeochemical differences between El Niño**
605 **and La Niña. During El Niño, lower primary productivy (green phytoplankton) and organic matter (brown**
606 **circles) accompany less upwelling and a deeper oxycline (dashed line), ultimately suppressing high N_2O**
607 **production. The opposite is true during La Niña, when the oxycline is upwelled and more organic matter**
608 **reaches low oxygen waters, leading to an increase in denitrification processes and greater N_2O accumilation**
609 **in near-surface waters.**

610 **4.6 Impact of ENSO Event Intensity on N_2O Cycling**

611 ENSO event strength (mild, moderate, or strong) has a significant influence on the net N_2O flux
612 to the atmosphere from the tropical Pacific ocean (Babbin et al., 2020). The data from the current study
613 allowed us to investigate how the relative intensity of an ENSO event influences the microbial sources of
614 N_2O and its accumulation from the oceanographic perspective. We did this by comparing our data to
615 other published N_2O concentrations and isotopocule data from a location approximately a half degree
616 longitude to the east of Station 11, during 2015, a strong El Niño year (Ji et al., 2019). Similarity in
617 accuracy of isotopic measurements between datasets was assessed by comparing N_2O isotopologues at
618 deepest common depth (1000 m). Measurements between datasets were comparable and any differences
619 were smaller than the difference in values between ENSO states.

The key N_2O concentration difference between the strong 2015 El Niño and the moderate 2010 El Niño is that in 2010, the [N_2O] maximum started at 100 m and stayed roughly at the same concentration (within 10 nM) until 200 m, where it then matched the 2015 data. In the upper 60 m of the water column, N_2O concentrations in the 2015 El Niño were more similar to our higher La Niña measurements than our 2010 El Niño measurements (Fig. S4A). The comparatively shallow oxycline in the 2010 El Niño likely allowed for N_2O production to occur closer to the surface, whereas the significantly depressed isopycnals and oxycline in 2015 (not shown) likely prevented strong N_2O production occurring in the upper 100 m.

The N_2O isotopic measurements during the strong El Niño followed similar trends to our moderate El Niño measurements in the upper 100 m at Station 11, although the values were offset. Generally, during both El Niño events, $\delta^{18}O\text{-}N_2O$ values were low (<45‰) and SP values decreased from the surface to 100 m (Fig. S4B). The Keeling model result (SP_{prod}) from the previous study in the 'N_2O peak' (45-500 m, 5-20 μM O_2, and NO_2^- < 1 μM) for all of their stations was also within 2‰ of our El Niño depth-integrated SP from 0-100 m and yielded the same $\delta^{18}O\text{-}N_2O$ as ours. Thus, we propose that lateral mixing from the more coastal OMZ where N_2O is being produced from denitrification is a more likely candidate for the low SP, in addition to an overprinting signal of local hybrid N_2O production, which would maintain the low $\delta^{18}O\text{-}N_2O$ (Fig. 6). This is in agreement with the findings from the earlier study (Ji et al., 2019). In contrast, incomplete denitrification and N_2O consumption likely contribute to the accumulation of N_2O in oxycline waters at Station 11 during La Niña, based on the elevated $\delta^{18}O\text{-}N_2O$ coincident with low $\delta^{15}N^{bulk}$ and $\delta^{15}N^{\beta}$ values. Comparing these findings with the results from a moderate and strong El Niño supports the hypothesis that denitrification plays a more significant role in the local cycling of N_2O during La Niña relative to El Niño.

Finally, it is noteworthy to highlight the global impact that enhanced upwelling, manifested through varying physical mechanisms, has on N_2O cycling. Here, we found mixed N_2O sources partially derived from NO_2^- to play a substantial role, likely due to the shallower oxycline interacting with a greater organic matter supply to fuel greater nitrification and denitrification rates (Fig. 7; Yang et al., 2017). Similarly, Babbin et al. (2021) found enhanced upwelling during La Niña in the South Pacific to expand the total volume of suboxic waters, leading to large increases to the region's overall N_2O flux to the atmosphere. Other recent studies in the Eastern Tropical North Pacific ODZ (Kelly et al., 2021; Monreal et al., 2022) and in the Tropical North Atlantic (Grundle et al., 2017) found the shoaling effects of eddies to increase total N_2O accumulation, with isotopocule signatures also pointing toward incomplete denitrification as a significant source. Further, the hypothesized upwelling of N_2O to more oxygenated waters from waters that previously experienced strong denitrification, were used to explain dramatic increases in $\delta^{18}O\text{-}N_2O$ and decreases in $\delta^{15}N^{\beta}$, of similar magnitudes to those observed in our study

(Bourbonnais et al., 2017). Thus, the interpreted effects of La Niña (or El Niño) on N_2O cycling and accumulation could be extended to other marine environments where extended periods of altered upwelling can occur.

5. Conclusion

Measurements of N_2O concentrations and isotopocules from the strong oxygen gradients in the ETSP demonstrate distinct sources of N_2O between moderate El Niño and La Niña events. During El Niño, increasing $\delta^{15}N^{\beta}$ and decreasing $\delta^{18}O$-N_2O and SP values throughout the top 100 m at Station 7 and above the oxyclines at Stations 9 and 11 suggest a role for hybrid N_2O in local N_2O production, overprinting a remote denitrification signal. In contrast, La Niña oxycline waters had marked decreases in $\delta^{15}N^{\beta}$ and increases in $\delta^{18}O$-N_2O and point toward incomplete denitrification as a significant source. Again, if non-traditional isotopic assumptions are introduced into our interpretation, such as N_2O production from incomplete denitrification having a positive SP or hybrid production having a lower SP, then the significantly enhanced N_2O accumulation could also be explained via those mechanisms (Casciotti et al., 2018; Kelly et al., 2021; Monreal et al., 2022). Isotope mixing models and Rayleigh models also indicate that N_2O consumption must be taking place at Station 11 during La Niña, but are not necessary at the other stations during either ENSO event. Our interpretations of N_2O cycling during a moderate El Niño were also tested against a strong El Niño, where findings were quite similar: N_2O in the oxycline and peak was being produced at low rates likely from a hybrid mechanism, but with other potential overprinting signals such as mixing from allochthonous sources from more coastal waters. Ultimately, during El Niño, we found significantly reduced N_2O accumulation at Stations 9 and 11 and atmospheric fluxes up to two orders of magnitude lower, as all water column properties were subducted, and lower rates of N_2O production were occurring in the upper 100 m. This work highlights the power of repeat measurements in the same region to resolve N_2O dynamics in distinct climate scenarios, such as the El Niño-Southern Oscillation, and the need to continue such work to better understand the response of N_2O cycling to climactically relevant alterations to ocean biogeochemistry and circulation. Through this exercise, we strongly recommend that future investigations also consider a range of potential SP values from incomplete denitrification and hybrid production, as sources of N_2O.

Supplementary Figures

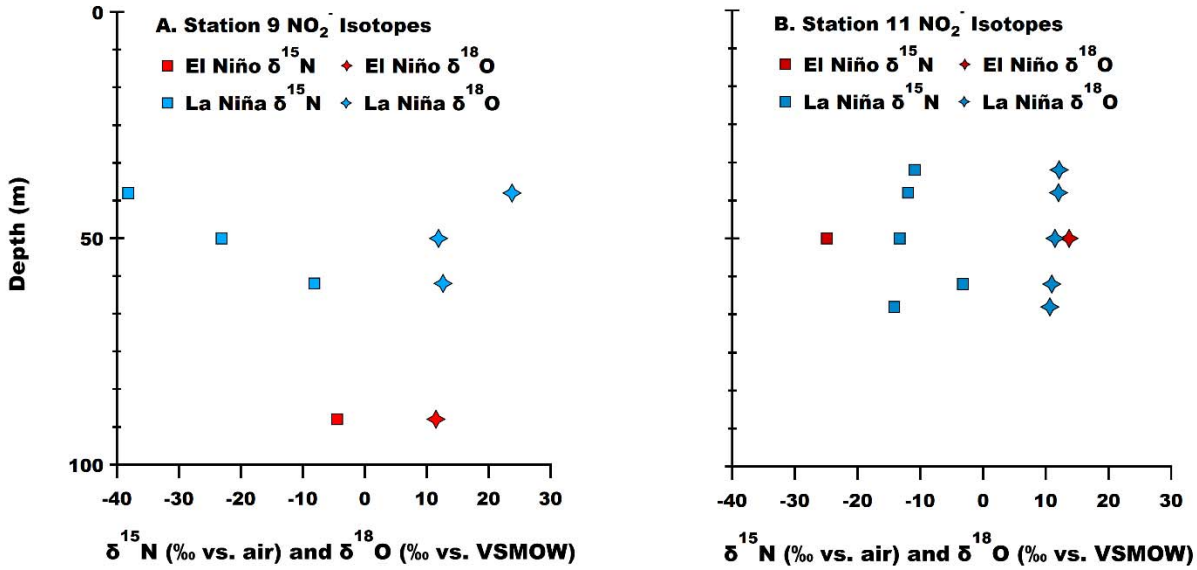

Figure S1: $\delta^{15}N\text{-}NO_2^-$ (squares) and $\delta^{18}O\text{-}NO_2^-$ (diamonds) at Station 9 (A) and Station 11 (B). El Niño (red) and La Niña (blue).

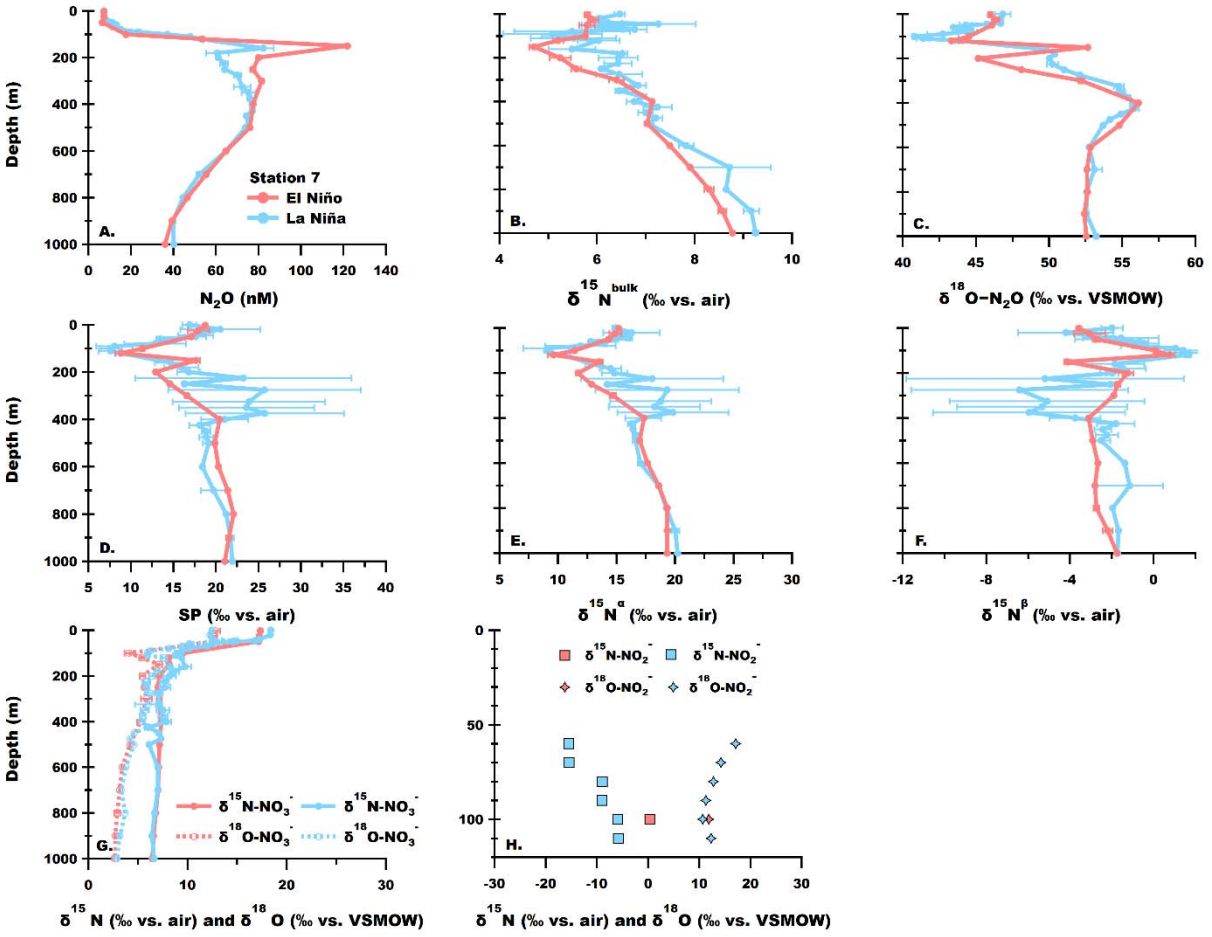

685

686 **Figure S2: Station 7 El Niño (red) and La Niña (blue) N_2O A) concentrations (nM); B) $\delta^{15}N^{bulk}$ (‰ vs. air); C)**
687 **$\delta^{18}O$-N_2O (‰ vs. VSMOW); D) SP (‰ vs. air); E) $\delta^{15}N^{\alpha}$ (‰ vs. air); F) $\delta^{15}N^{\beta}$ (‰ vs. air); G) $\delta^{15}N$-NO_3^- (filled**
688 **circles, solid line) and $\delta^{18}O$-NO_3^- (open circles, dashed line); and H) $\delta^{15}N$-NO_2^- (filled squares) and $\delta^{18}O$-NO_2^-**
689 **(filled diamonds) illustrated.**

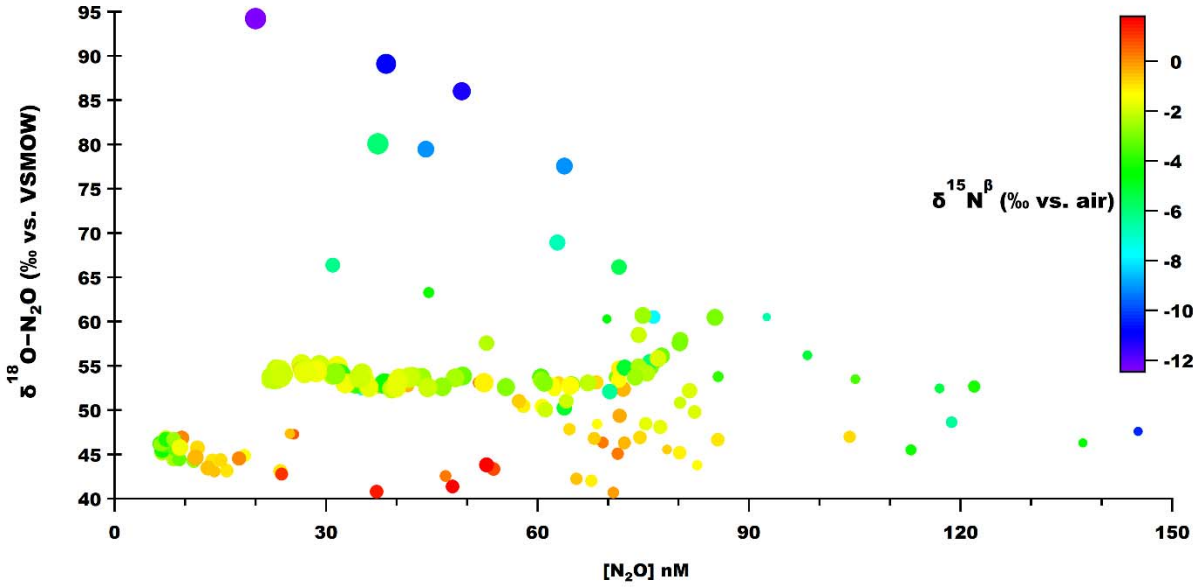

690

691 **Figure S3: $\delta^{18}O$-N_2O versus [N_2O] plotted for all Stations 7, 9, and 11 measurements. Marker color is a**

692 **function of $\delta^{15}N^{\beta}$ and marker size is a function of $\delta^{15}N^{bulk}$.**

693

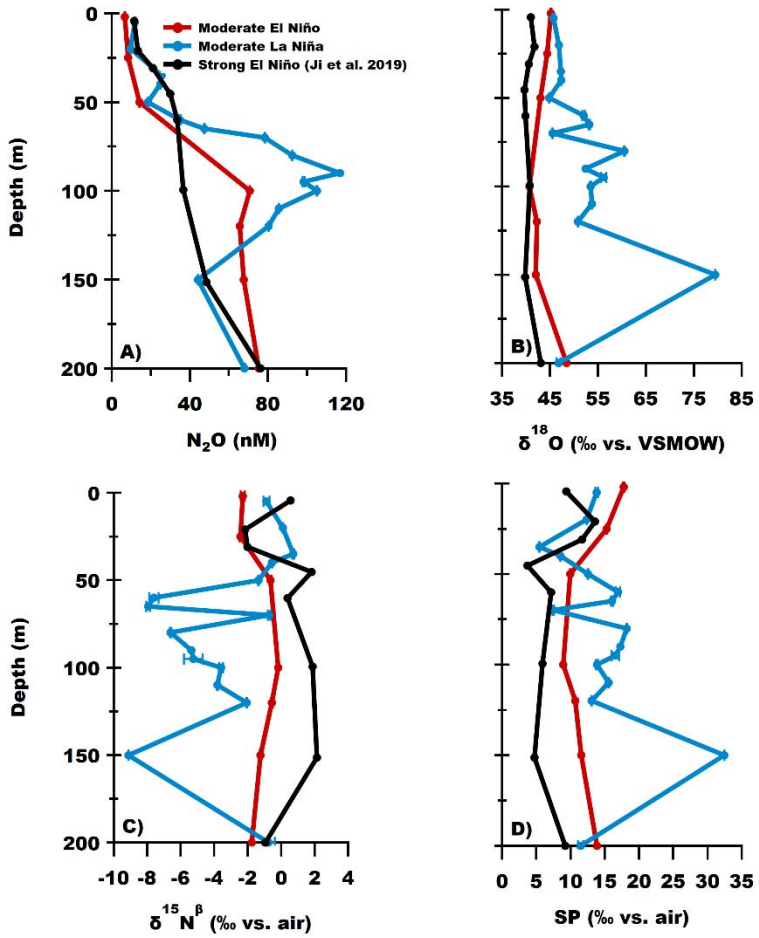

Figure S4: N_2O A) concentrations (nM); B) $\delta^{18}O$-N_2O (‰ vs. VSMOW); C) $\delta^{15}N^{\beta}$ (‰ vs. air); D) SP (‰ vs. air) illustrated for Station 11 and nearby station from Ji et al. (2019). Our data from a moderate El Niño (red) and La Niña (blue) are shown along with the strong 2015 El Niño N_2O data (black; Ji et al., 2019). Most apparent differences between values occur from the oxycline (50 m) into the ODZ (200 m) from both El Niño events, compared to the La Niña.

Offset Correction (‰)	$\delta^{15}N^{\alpha}$	$\delta^{15}N^{\beta}$	SP	$\delta^{15}N^{bulk}$	$\delta^{18}O$-N_2O
2012	-0.37	-0.20	-0.17	-0.28	-1.65
2014	-0.25	-0.96	0.71	-0.61	-0.29
2017	-1.37	-1.53	0.16	-1.35	-1.80

Table S1: Offset correction performed on 2011 dataset using differences against 2010 deep water (1000 m-3000 m). Individual corrections were made for each isotopic variable of N_2O for a given analysis year due to annual variability.

6. References

Arévalo-Martínez, D. L., Kock, A., Löscher, C. R., Schmitz, R. A., & Bange, H. W. (2015). Massive nitrous oxide emissions from the tropical South Pacific Ocean. *Nature Geoscience*, *8*(7), 530–533. https://doi.org/10.1038/ngeo2469

Babbin, A. R., Bianchi, D., Jayakumar, A., & Ward, B. B. (2015). Rapid nitrous oxide cycling in the suboxic ocean. *Science*, *348*(6239), 1127–1129. https://doi.org/10.1126/science.aaa8380

Babbin, A. R., Boles, E. L., Mühle, J., & Weiss, R. F. (2020). On the natural spatio-temporal heterogeneity of South Pacific nitrous oxide. *Nature Communications*, *11*(1), 3672. https://doi.org/10.1038/s41467-020-17509-6

Berelson, W. M., Haskell, W. Z., Prokopenko, M., Knapp, A. N., Hammond, D. E., Rollins, N., & Capone, D. G. (2015). Biogenic particle flux and benthic remineralization in the Eastern Tropical South Pacific. *Deep Sea Research Part I: Oceanographic Research Papers*, *99*, 23–34. https://doi.org/10.1016/j.dsr.2014.12.006

Bonin, P., Gilewicz, M., & Bertrand, J. C. (1989). Effects of oxygen on each step of denitrification on *Pseudomonas nautica*. *Canadian Journal of Microbiology*, *35*(11), 1061–1064. https://doi.org/10.1139/m89-177

Bourbonnais, A., Altabet, M. A., Charoenpong, C. N., Larkum, J., Hu, H., Bange, H. W., & Stramma, L. (2015). N-loss isotope effects in the Peru oxygen minimum zone studied using a mesoscale eddy as a natural tracer experiment. *Global Biogeochemical Cycles*, *29*(6), 793–811. https://doi.org/10.1002/2014GB005001

Bourbonnais, A., Letscher, R. T., Bange, H. W., Échevin, V., Larkum, J., Mohn, J., Yoshida, N., & Altabet, M. A. (2017). N_2O production and consumption from stable isotopic and concentration data in the Peruvian coastal upwelling system: N_2O Production and Consumption off Peru. *Global Biogeochemical Cycles*, *31*(4), 678–698. https://doi.org/10.1002/2016GB005567

Bulow, S. E., Rich, J. J., Naik, H. S., Pratihary, A. K., & Ward, B. B. (2010). Denitrification exceeds anammox as a nitrogen loss pathway in the Arabian Sea oxygen minimum zone. *Deep Sea Research Part I: Oceanographic Research Papers*, *57*(3), 384–393. https://doi.org/10.1016/j.dsr.2009.10.014

Cai, W., Borlace, S., Lengaigne, M., van Rensch, P., Collins, M., Vecchi, G., Timmermann, A., Santoso, A., McPhaden, M. J., Wu, L., England, M. H., Wang, G., Guilyardi, E., & Jin, F.-F. (2014). Increasing frequency of extreme El Niño events due to greenhouse warming. *Nature Climate Change*, *4*(2), 111–116. https://doi.org/10.1038/nclimate2100

Cai, W., Wang, G., Santoso, A., McPhaden, M. J., Wu, L., Jin, F.-F., Timmermann, A., Collins, M., Vecchi, G., Lengaigne, M., England, M. H., Dommenget, D., Takahashi, K., & Guilyardi, E. (2015). Increased frequency of extreme La Niña events under greenhouse warming. *Nature Climate Change*, *5*(2), 132–137. https://doi.org/10.1038/nclimate2492

Casciotti, K. L. (2009). Inverse kinetic isotope fractionation during bacterial nitrite oxidation. *Geochimica et Cosmochimica Acta*, *73*(7), 2061–2076. https://doi.org/10.1016/j.gca.2008.12.022

Casciotti, K. L., Böhlke, J. K., McIlvin, M. R., Mroczkowski, S. J., & Hannon, J. E. (2007). Oxygen Isotopes in Nitrite: Analysis, Calibration, and Equilibration. *Analytical Chemistry*, *79*(6), 2427–2436. https://doi.org/10.1021/ac061598h

Casciotti, K. L., Forbes, M., Vedamati, J., Peters, B. D., Martin, T. S., & Mordy, C. W. (2018). Nitrous oxide cycling in the Eastern Tropical South Pacific as inferred from isotopic and isotopomeric data. *Deep Sea Research Part II: Topical Studies in Oceanography*, *156*, 155–167. https://doi.org/10.1016/j.dsr2.2018.07.014

Casciotti, K. L., Sigman, D. M., Hastings, M. G., Böhlke, J. K., & Hilkert, A. (2002). Measurement of the Oxygen Isotopic Composition of Nitrate in Seawater and Freshwater Using the Denitrifier Method. *Analytical Chemistry*, *74*(19), 4905–4912. https://doi.org/10.1021/ac020113w

Cohen, Y., & Gordon, L. I. (1978). Nitrous oxide in the oxygen minimum of the eastern tropical North Pacific: Evidence for its consumption during denitrification and possible mechanisms for its production. *Deep Sea Research*, *25*(6), 509–524. https://doi.org/10.1016/0146-6291(78)90640-9

Crutzen, P. J. (1970). The influence of nitrogen oxides on the atmospheric ozone content. *Quarterly Journal of the Royal Meteorological Society*, *96*(408), 320–325. https://doi.org/10.1002/qj.49709640815

Elkins, J. W., Wofsy, S. C., McElroy, M. B., Kolb, C. E., & Kaplan, W. A. (1978). Aquatic sources and sinks for nitrous oxide. *Nature*, *275*(5681), Article 5681. https://doi.org/10.1038/275602a0

Espinoza-Morriberón, D., Echevin, V., Colas, F., Tam, J., Gutierrez, D., Graco, M., Ledesma, J., & Quispe-Ccalluari, C. (2019). Oxygen Variability During ENSO in the Tropical South Eastern Pacific. *Frontiers in Marine Science*, *5*, 526. https://doi.org/10.3389/fmars.2018.00526

Farías, L., Castro-González, M., Cornejo, M., Charpentier, J., Faúndez, J., Boontanon, N., & Yoshida, N. (2009). Denitrification and nitrous oxide cycling within the upper oxycline of the eastern tropical South Pacific oxygen minimum zone. *Limnology and Oceanography*, *54*(1), 132–144. https://doi.org/10.4319/lo.2009.54.1.0132

Frame, C. H., & Casciotti, K. L. (2010). Biogeochemical controls and isotopic signatures of nitrous oxide production by a marine ammonia-oxidizing bacterium. *Biogeosciences*, *7*(9), 2695–2709. https://doi.org/10.5194/bg-7-2695-2010

Frame, C. H., Deal, E., Nevison, C. D., & Casciotti, K. L. (2014). N2O production in the eastern South Atlantic: Analysis of N2O stable isotopic and concentration data. *Global Biogeochemical Cycles*, *28*(11), 1262–1278. https://doi.org/10.1002/2013GB004790

780 Frame, C. H., Lau, E., Nolan, E. J. I., Goepfert, T. J., & Lehmann, M. F. (2017). Acidification Enhances
781 Hybrid N2O Production Associated with Aquatic Ammonia-Oxidizing Microorganisms.
782 *Frontiers in Microbiology*, *7*. https://doi.org/10.3389/fmicb.2016.02104
783 Francis, C. A., Roberts, K. J., Beman, J. M., Santoro, A. E., & Oakley, B. B. (2005). Ubiquity and
784 diversity of ammonia-oxidizing archaea in water columns and sediments of the ocean.
785 *Proceedings of the National Academy of Sciences*, *102*(41), 14683–14688.
786 https://doi.org/10.1073/pnas.0506625102
787 Frey, C., Bange, H. W., Achterberg, E. P., Jayakumar, A., Löscher, C. R., Arévalo-Martínez, D. L., León-
788 Palmero, E., Sun, M., Sun, X., Xie, R. C., Oleynik, S., & Ward, B. B. (2020). Regulation of
789 nitrous oxide production in low-oxygen waters off the coast of Peru. *Biogeosciences*, *17*(8),
790 2263–2287. https://doi.org/10.5194/bg-17-2263-2020
791 Fuenzalida, R., Schneider, W., Garcés-Vargas, J., Bravo, L., & Lange, C. (2009). Vertical and horizontal
792 extension of the oxygen minimum zone in the eastern South Pacific Ocean. *Deep Sea Research*
793 *Part II: Topical Studies in Oceanography*, *56*(16), 992–1003.
794 https://doi.org/10.1016/j.dsr2.2008.11.001
795 Fujii, A., Toyoda, S., Yoshida, O., Watanabe, S., Sasaki, K., & Yoshida, N. (2013). Distribution of
796 nitrous oxide dissolved in water masses in the eastern subtropical North Pacific and its origin
797 inferred from isotopomer analysis. *Journal of Oceanography*, *69*(2), 147–157.
798 https://doi.org/10.1007/s10872-012-0162-4
799 Granger, J., & Sigman, D. M. (2009). Removal of nitrite with sulfamic acid for nitrate N and O isotope
800 analysis with the denitrifier method. *Rapid Communications in Mass Spectrometry*, *23*(23), 3753–
801 3762. https://doi.org/10.1002/rcm.4307
802 Grundle, D. S., Löscher, C. R., Krahmann, G., Altabet, M. A., Bange, H. W., Karstensen, J., Körtzinger,
803 A., & Fiedler, B. (2017). Low oxygen eddies in the eastern tropical North Atlantic: Implications
804 for N2O cycling. *Scientific Reports*, *7*(1), 4806. https://doi.org/10.1038/s41598-017-04745-y

Haskell, W. Z., Berelson, W. M., Hammond, D. E., & Capone, D. G. (2013). Particle sinking dynamics and POC fluxes in the Eastern Tropical South Pacific based on 234Th budgets and sediment trap deployments. *Deep Sea Research Part I: Oceanographic Research Papers*, *81*, 1–13. https://doi.org/10.1016/j.dsr.2013.07.001

Haskell, W. Z., Kadko, D., Hammond, D. E., Knapp, A. N., Prokopenko, M. G., Berelson, W. M., & Capone, D. G. (2015). Upwelling velocity and eddy diffusivity from 7Be measurements used to compare vertical nutrient flux to export POC flux in the Eastern Tropical South Pacific. *Marine Chemistry*, *168*, 140–150. https://doi.org/10.1016/j.marchem.2014.10.004

Horak, R. E. A., Ruef, W., Ward, B. B., & Devol, A. H. (2016). Expansion of denitrification and anoxia in the eastern tropical North Pacific from 1972 to 2012. *Geophysical Research Letters*, *43*(10), 5252–5260. https://doi.org/10.1002/2016GL068871

Ji, Q., Altabet, M. A., Bange, H. W., Graco, M. I., Ma, X., Arévalo-Martínez, D. L., & Grundle, D. S. (2019). Investigating the effect of El Niño on nitrous oxide distribution in the eastern tropical South Pacific. *Biogeosciences*, *16*(9), 2079–2093. https://doi.org/10.5194/bg-16-2079-2019

Ji, Q., Babbin, A. R., Jayakumar, A., Oleynik, S., & Ward, B. B. (2015). Nitrous oxide production by nitrification and denitrification in the Eastern Tropical South Pacific oxygen minimum zone: NITROUS OXIDE PRODUCTION IN OMZ. *Geophysical Research Letters*, *42*(24), 10,755-10,764. https://doi.org/10.1002/2015GL066853

Ji, Q., Buitenhuis, E., Suntharalingam, P., Sarmiento, J. L., & Ward, B. B. (2018). Global Nitrous Oxide Production Determined by Oxygen Sensitivity of Nitrification and Denitrification. *Global Biogeochemical Cycles*, *32*(12), 1790–1802. https://doi.org/10.1029/2018GB005887

Jung, M.-Y., Well, R., Min, D., Giesemann, A., Park, S.-J., Kim, J.-G., Kim, S.-J., & Rhee, S.-K. (2014). Isotopic signatures of N2O produced by ammonia-oxidizing archaea from soils. *The ISME Journal*, *8*(5), Article 5. https://doi.org/10.1038/ismej.2013.205

Kelly, C. L., Travis, N. M., Baya, P. A., & Casciotti, K. L. (2021). Quantifying Nitrous Oxide Cycling Regimes in the Eastern Tropical North Pacific Ocean With Isotopomer Analysis. *Global Biogeochemical Cycles*, *35*(2), e2020GB006637. https://doi.org/10.1029/2020GB006637

Knapp, A. N., Casciotti, K. L., Berelson, W. M., Prokopenko, M. G., & Capone, D. G. (2016). Low rates of nitrogen fixation in eastern tropical South Pacific surface waters. *Proceedings of the National Academy of Sciences*, *113*(16), 4398–4403. https://doi.org/10.1073/pnas.1515641113

Kozlowski, J. A., Kits, K. D., & Stein, L. Y. (2016). Comparison of Nitrogen Oxide Metabolism among Diverse Ammonia-Oxidizing Bacteria. *Frontiers in Microbiology*, *7*, 1090. https://doi.org/10.3389/fmicb.2016.01090

Kuypers, M. M. M., Lavik, G., Woebken, D., Schmid, M., Fuchs, B. M., Amann, R., Jørgensen, B. B., & Jetten, M. S. M. (2005). Massive nitrogen loss from the Benguela upwelling system through anaerobic ammonium oxidation. *Proceedings of the National Academy of Sciences*, *102*(18), 6478–6483. https://doi.org/10.1073/pnas.0502088102

Llanillo, P. J., Karstensen, J., Pelegrí, J. L., & Stramma, L. (2013). Physical and biogeochemical forcing of oxygen and nitrate changes during El Niño/El Viejo and La Niña/La Vieja upper-ocean phases in the tropical eastern South Pacific along 86° W. *Biogeosciences (BG)*, *10*, 6339–6355. https://doi.org/10.5194/bg-10-6339-2013

Löscher, C. R., Kock, A., Könneke, M., LaRoche, J., Bange, H. W., & Schmitz, R. A. (2012). Production of oceanic nitrous oxide by ammonia-oxidizing archaea. *Biogeosciences*, *9*(7), 2419–2429. https://doi.org/10.5194/bg-9-2419-2012

Maeda, K., Spor, A., Edel-Hermann, V., Heraud, C., Breuil, M.-C., Bizouard, F., Toyoda, S., Yoshida, N., Steinberg, C., & Philippot, L. (2015). N2O production, a widespread trait in fungi. *Scientific Reports*, *5*(1), 9697. https://doi.org/10.1038/srep09697

Martin, T. S., & Casciotti, K. L. (2016). Nitrogen and oxygen isotopic fractionation during microbial nitrite reduction. *Limnology and Oceanography*, *61*(3), 1134–1143. https://doi.org/10.1002/lno.10278

Martinez-Rey, J., Bopp, L., Gehlen, M., Tagliabue, A., & Gruber, N. (2015). Projections of oceanic N₂O emissions in the 21st century using the IPSL Earth system model. *Biogeosciences*, *12*(13), 4133–4148. https://doi.org/10.5194/bg-12-4133-2015

McIlvin, M. R., & Altabet, M. A. (2005). Chemical conversion of nitrate and nitrite to nitrous oxide for nitrogen and oxygen isotopic analysis in freshwater and seawater. *Analytical Chemistry*, *77*(17), 5589–5595. https://doi.org/10.1021/ac050528s

McIlvin, M. R., & Casciotti, K. L. (2010). Fully automated system for stable isotopic analyses of dissolved nitrous oxide at natural abundance levels. *Limnology and Oceanography: Methods*, *8*(2), 54–66. https://doi.org/10.4319/lom.2010.8.54

Mogollón, R., & Calil, P. H. R. (2017). On the effects of ENSO on ocean biogeochemistry in the Northern Humboldt Current System (NHCS): A modeling study. *Journal of Marine Systems*, *172*, 137–159. https://doi.org/10.1016/j.jmarsys.2017.03.011

Mohn, J., Wolf, B., Toyoda, S., Lin, C.-T., Liang, M.-C., Brüggemann, N., Wissel, H., Steiker, A. E., Dyckmans, J., Szwec, L., Ostrom, N. E., Casciotti, K. L., Forbes, M., Giesemann, A., Well, R., Doucett, R. R., Yarnes, C. T., Ridley, A. R., Kaiser, J., & Yoshida, N. (2014). Interlaboratory assessment of nitrous oxide isotopomer analysis by isotope ratio mass spectrometry and laser spectroscopy: Current status and perspectives: Interlaboratory assessment of nitrous oxide isotopomer analysis. *Rapid Communications in Mass Spectrometry*, *28*(18), 1995–2007. https://doi.org/10.1002/rcm.6982

Monreal, P. J., Kelly, C. L., Travis, N. M., & Casciotti, K. L. (2022). Identifying the Sources and Drivers of Nitrous Oxide Accumulation in the Eddy-Influenced Eastern Tropical North Pacific Oxygen-Deficient Zone. *Global Biogeochemical Cycles*, *36*(6), e2022GB007310. https://doi.org/10.1029/2022GB007310

National Centers for Environmental Prediction, National Weather Service, NOAA, U.S. Department of Commerce. (2000). *NCEP/DOE Reanalysis 2 (R2)*. Research Data Archive at the National Center

for Atmospheric Research, Computational and Information Systems Laboratory. https://doi.org/10.5065/KVQZ-YJ93

Nevison, C. D., Butler, J. H., & Elkins, J. W. (2003). Global distribution of N_2O and the ΔN_2O-AOU yield in the subsurface ocean. *Global Biogeochemical Cycles*, *17*(4), n/a-n/a. https://doi.org/10.1029/2003GB002068

Nevison, C. D., Lueker, T. J., & Weiss, R. F. (2004). Quantifying the nitrous oxide source from coastal upwelling: N_2O FROM COASTAL UPWELLING. *Global Biogeochemical Cycles*, *18*(1), n/a-n/a. https://doi.org/10.1029/2003GB002110

NOAA's Climate Prediction Center. (n.d.). *NOAA's Climate Prediction Center*. Retrieved November 21, 2021, from https://origin.cpc.ncep.noaa.gov/products/analysis_monitoring/ensostuff/ONI_v5.php

Ostrom, N. E., Pitt, A., Sutka, R., Ostrom, P. H., Grandy, A. S., Huizinga, K. M., & Robertson, G. P. (2007). Isotopologue effects during N_2O reduction in soils and in pure cultures of denitrifiers. *Journal of Geophysical Research*, *112*(G2), G02005. https://doi.org/10.1029/2006JG000287

Peng, X., & Valentine, D. L. (2021). Diversity and N2O Production Potential of Fungi in an Oceanic Oxygen Minimum Zone. *Journal of Fungi*, *7*(3), Article 3. https://doi.org/10.3390/jof7030218

Ravishankara, A. R., Daniel, J. S., & Portmann, R. W. (2009). Nitrous Oxide (N2O): The Dominant Ozone-Depleting Substance Emitted in the 21st Century. *Science*, *326*(5949), 123–125. https://doi.org/10.1126/science.1176985

Rohe, L., Anderson, T.-H., Braker, G., Flessa, H., Giesemann, A., Lewicka-Szczebak, D., Wrage-Mönnig, N., & Well, R. (2014). Dual isotope and isotopomer signatures of nitrous oxide from fungal denitrification – a pure culture study. *Rapid Communications in Mass Spectrometry*, *28*(17), 1893–1903. https://doi.org/10.1002/rcm.6975

Santoro, A. E., Buchwald, C., Knapp, A. N., Berelson, W. M., Capone, D. G., & Casciotti, K. L. (2021). Nitrification and Nitrous Oxide Production in the Offshore Waters of the Eastern Tropical South Pacific. *Global Biogeochemical Cycles*, *35*(2), e2020GB006716. https://doi.org/10.1029/2020GB006716

Santoro, A. E., Buchwald, C., McIlvin, M. R., & Casciotti, K. L. (2011). Isotopic Signature of N_2O Produced by Marine Ammonia-Oxidizing Archaea. *Science*, *333*(6047), 1282–1285. https://doi.org/10.1126/science.1208239

Santoro, A. E., Casciotti, K. L., & Francis, C. A. (2010). Activity, abundance and diversity of nitrifying archaea and bacteria in the central California Current. *Environmental Microbiology*, *12*(7), 1989–2006. https://doi.org/10.1111/j.1462-2920.2010.02205.x

Schmidt, H.-L., Werner, R. A., Yoshida, N., & Well, R. (2004). Is the isotopic composition of nitrous oxide an indicator for its origin from nitrification or denitrification? A theoretical approach from referred data and microbiological and enzyme kinetic aspects. *Rapid Communications in Mass Spectrometry*, *18*(18), 2036–2040. https://doi.org/10.1002/rcm.1586

Schmidtko, S., Stramma, L., & Visbeck, M. (2017). Decline in global oceanic oxygen content during the past five decades. *Nature*, *542*(7641), 335–339. https://doi.org/10.1038/nature21399

Sigman, D. M., Casciotti, K. L., Andreani, M., Barford, C., Galanter, M., & Böhlke, J. K. (2001). A Bacterial Method for the Nitrogen Isotopic Analysis of Nitrate in Seawater and Freshwater. *Analytical Chemistry*, *73*(17), 4145–4153. https://doi.org/10.1021/ac010088e

Stein, L. Y. (2019). Insights into the physiology of ammonia-oxidizing microorganisms. *Current Opinion in Chemical Biology*, *49*, 9–15. https://doi.org/10.1016/j.cbpa.2018.09.003

Stieglmeier, M., Mooshammer, M., Kitzler, B., Wanek, W., Zechmeister-Boltenstern, S., Richter, A., & Schleper, C. (2014). Aerobic nitrous oxide production through N-nitrosating hybrid formation in ammonia-oxidizing archaea. *The ISME Journal*, *8*(5), 1135–1146. https://doi.org/10.1038/ismej.2013.220

Stramma, L., Johnson, G. C., Sprintall, J., & Mohrholz, V. (2008). Expanding Oxygen-Minimum Zones in the Tropical Oceans. *Science*, *320*(5876), 655–658. https://doi.org/10.1126/science.1153847

Sun, X., Jayakumar, A., Tracey, J., Wallace, E., Kelly, C., Casciotti, K., & Ward, B. (2020). Microbial N2O consumption in and above marine N2O production hotspots. *The ISME Journal*. https://doi.org/10.1038/s41396-020-00861-2

Suntharalingam, P., & Sarmiento, J. L. (2000). Factors governing the oceanic nitrous oxide distribution: Simulations with an ocean general circulation model. *Global Biogeochemical Cycles*, *14*(1), 429–454. https://doi.org/10.1029/1999GB900032

Sutka, R. L., Adams, G. C., Ostrom, N. E., & Ostrom, P. H. (2008). Isotopologue fractionation during N2O production by fungal denitrification. *Rapid Communications in Mass Spectrometry*, *22*(24), 3989–3996. https://doi.org/10.1002/rcm.3820

Sutka, R. L., Ostrom, N. E., Ostrom, P. H., Breznak, J. A., Gandhi, H., Pitt, A. J., & Li, F. (2006). Distinguishing Nitrous Oxide Production from Nitrification and Denitrification on the Basis of Isotopomer Abundances. *Applied and Environmental Microbiology*, *72*(1), 638–644. https://doi.org/10.1128/AEM.72.1.638-644.2006

Thompson, R. L., Chevallier, F., Crotwell, A. M., Dutton, G., Langenfelds, R. L., Prinn, R. G., Weiss, R. F., Tohjima, Y., Nakazawa, T., Krummel, P. B., Steele, L. P., Fraser, P., O'Doherty, S., Ishijima, K., & Aoki, S. (2014). Nitrous oxide emissions 1999 to 2009 from a global atmospheric inversion. *Atmospheric Chemistry and Physics*, *14*(4), 1801–1817. https://doi.org/10.5194/acp-14-1801-2014

Thompson, R. L., Lassaletta, L., Patra, P. K., Wilson, C., Wells, K. C., Gressent, A., Koffi, E. N., Chipperfield, M. P., Winiwarter, W., Davidson, E. A., Tian, H., & Canadell, J. G. (2019). Acceleration of global N2O emissions seen from two decades of atmospheric inversion. *Nature Climate Change*, *9*(12), 993–998. https://doi.org/10.1038/s41558-019-0613-7

Tian, H., Xu, R., Canadell, J. G., Thompson, R. L., Winiwarter, W., Suntharalingam, P., Davidson, E. A., Ciais, P., Jackson, R. B., Janssens-Maenhout, G., Prather, M. J., Regnier, P., Pan, N., Pan, S., Peters, G. P., Shi, H., Tubiello, F. N., Zaehle, S., Zhou, F., … Yao, Y. (2020). A comprehensive quantification of global nitrous oxide sources and sinks. *Nature*, *586*(7828), 248–256. https://doi.org/10.1038/s41586-020-2780-0

Toyoda, S. (2002). Production mechanism and global budget of N_2O inferred from its isotopomers in the western North Pacific. *Geophysical Research Letters*, *29*(3), 1037. https://doi.org/10.1029/2001GL014311

Toyoda, S., Mutobe, H., Yamagishi, H., Yoshida, N., & Tanji, Y. (2005). Fractionation of N2O isotopomers during production by denitrifier. *Soil Biology and Biochemistry*, *37*(8), 1535–1545. https://doi.org/10.1016/j.soilbio.2005.01.009

Toyoda, S., & Yoshida, N. (1999). Determination of Nitrogen Isotopomers of Nitrous Oxide on a Modified Isotope Ratio Mass Spectrometer. *Analytical Chemistry*, *71*(20), 4711–4718. https://doi.org/10.1021/ac9904563

Wanninkhof, R. (2014). Relationship between wind speed and gas exchange over the ocean revisited. *Limnology and Oceanography: Methods*, *12*(6), 351–362. https://doi.org/10.4319/lom.2014.12.351

Ward, B. B., Devol, A. H., Rich, J. J., Chang, B. X., Bulow, S. E., Naik, H., Pratihary, A., & Jayakumar, A. (2009). Denitrification as the dominant nitrogen loss process in the Arabian Sea. *Nature*, *461*(7260), 78–81. https://doi.org/10.1038/nature08276

Weiss, R. F., & Price, B. A. (1980). Nitrous oxide solubility in water and seawater. *Marine Chemistry*, *8*(4), 347–359. https://doi.org/10.1016/0304-4203(80)90024-9

Yamagishi, H., Westley, M. B., Popp, B. N., Toyoda, S., Yoshida, N., Watanabe, S., Koba, K., & Yamanaka, Y. (2007). Role of nitrification and denitrification on the nitrous oxide cycle in the eastern tropical North Pacific and Gulf of California. *Journal of Geophysical Research: Biogeosciences*, *112*(G2). https://doi.org/10.1029/2006JG000227

Yang, S., Chang, B. X., Warner, M. J., Weber, T. S., Bourbonnais, A. M., Santoro, A. E., Kock, A., Sonnerup, R. E., Bullister, J. L., Wilson, S. T., & Bianchi, D. (2020). Global reconstruction reduces the uncertainty of oceanic nitrous oxide emissions and reveals a vigorous seasonal cycle. *Proceedings of the National Academy of Sciences*, *117*(22), 11954–11960. https://doi.org/10.1073/pnas.1921914117

Yang, S., Gruber, N., Long, M. C., & Vogt, M. (2017). ENSO-Driven Variability of Denitrification and Suboxia in the Eastern Tropical Pacific Ocean: ENSO, DENITRIFICATION AND SUBOXIA. *Global Biogeochemical Cycles*, *31*(10), 1470–1487. https://doi.org/10.1002/2016GB005596

Yoshinari, T. (1976). Nitrous oxide in the sea. *Marine Chemistry*, *4*(2), 189–202. https://doi.org/10.1016/0304-4203(76)90007-4